RADIATION TRANSPORT
CROSS-SECTION SENSITIVITY ANALYSIS —
A GENERAL APPROACH ILLUSTRATED
FOR A THERMONUCLEAR SOURCE IN AIR

D. E. Bartine
E. M. Oblow
F. R. Mynatt

OAK RIDGE NATIONAL LABORATORY

Contract No. W-7405-eng-26

Neutron Physics Division

RADIATION TRANSPORT
CROSS-SECTION SENSITIVITY ANALYSIS - A GENERAL APPROACH
ILLUSTRATED FOR A THERMONUCLEAR SOURCE IN AIR

D. E. Bartine*

E. M. Oblow   F. R. Mynatt

*Computer Science Division

DECEMBER 1973

NOTE:

OAK RIDGE NATIONAL LABORATORY
Oak Ridge, Tennessee   37830
operated by
UNION CARBIDE CORPORATION
for the
U. S. ATOMIC ENERGY COMMISSION

TABLE OF CONTENTS

LIST OF FIGURES

LIST OF TABLES

ABSTRACT

A general approach to radiation transport cross-section sensitivity analysis is introduced and its applicability demonstrated for a problem involving neutron and gamma-ray transport in air. The basis for the method is generalized perturbation theory using flux solutions to the transport equation and its adjoint. Both an analytical aspect of the technique, designed for surveying the sensitivity of a result to the entire cross-section data field, and a predictive aspect, designed for predicting the effect of changes in the data field, are presented. The analytic procedure is demonstrated by results that include a determination of important energy regions in the total, partial, and gamma-ray-production cross sections of nitrogen and oxygen for deep-penetration calculations of tissue dose in air. The predictive capability is illustrated for specific cross-section perturbations in the system and the effects of truncating the Legendre expansion of the scattering kernel. In addition, the applicability of the method for predicting variances in a calculated result arising from cross-section data uncertainties is demonstrated. In the sample case, the variance in the total neutron-gamma tissue dose is estimated from preliminary cross-section error files given in the evaluations of the nitrogen and oxygen cross sections.

BLANK PAGE

I. INTRODUCTION

Cross-section sensitivity analysis, the procedure by which one determines how sensitive a calculated result is to cross-section data, is finding increasing applicability in the areas of radiation shielding,[1-3] reactor physics,[4,5] and fusion reactor blanket studies.[6-8] While approaches to the problem vary considerably from application to application, ranging from direct data manipulation techniques [9-11] to the use of variational and perturbation theory,[12-15] all are basically attempting to find out what cross sections are most important in a given problem and what impact data uncertainties have on calculated results. The answers to these questions provide valuable information which can be used in guiding cross-section measurement and evaluation efforts as well as aiding reactor designers and safety engineers.

In attempting to determine cross-section data needs and the impact of data uncertainties on design problems, our approach has been to concentrate on the survey aspect of sensitivity analysis and easily implemented methods for estimating changes in calculated results based on cross-section changes. Both are essential ingredients in any approach which is to make quantitative assessments of the quality of so large a data base as exists for neutron and gamma-ray cross sections. The survey aspect of a sensitivity study is analytic in nature, describing in a qualitative and quantitative fashion the importance of each element in the entire cross-section data field used in solving a particular problem. Error estimates, on the other hand, require a predictive capability and ways of handling the statistical and correlated nature of cross-section data uncertainties. Additionally, in all aspects of analysis, it is important to recognize the problem-dependent nature of any study. The analysis must be tied strongly to a particular problem and specific calculated results for sensitivity to have any quantitative meaning.

With these considerations in mind, an approach to sensitivity analysis has been developed stressing both analytic and predictive capabilities. This approach relies heavily on perturbation theory as a most efficient

means of surveying large amounts of data with rather simple calculations.
A great deal of effort has gone into extending the use of the bilinear
functionals (quantities computed from products of the flux and its adjoint)
in perturbation theory to include an analytic capability. Here, use is
made of the physical interpretation of the adjoint flux as an importance
function. This leads to a physically meaningful definition of the term
"sensitivity" and useful quantitative definitions of the importance of
cross sections in a given problem.

It is tacitly assumed throughout this work that sensitivity questions
are properly stated only after all problem specifications are provided,
including sources, geometry, materials and detector responses. Sensitivity
questions for which quantitative answers are to be provided are therefore
strictly problem dependent. Generalizations from a particular study should
be very cautiously applied. Also assumed is the adequacy of linear predictive
approaches for estimating changes in the problem results arising from data
perturbations. This assumption is necessary if rigorous estimates of
mathematical variances for calculated results are to be easily made based
on the variances in the cross-section data. Since these latter variances
are based on statistical uncertainties in the basic data with definite
cross correlations between various elements of the data field, actual
perturbed data sets in statistically sufficient numbers would be needed
to estimate problem variances if non-linear effects were taken into
account.

In the following sections, the basic approach will be defined,
mathematically developed, and physically interpreted; an application
of the method for an air-transport problem in which both analytic and
predictive capabilities are demonstrated will be presented; and conclusion
and possible extensions offered.

II. THEORY

A. Definitions

To reduce the potential size of a sensitivity study to manageable proportions, to quantify the results, and in addition, to be able to draw from well-known mathematical formalisms, two basic elements of nomenclature must first be defined. In particular, the term "result" and "sensitivity" must be mathematically precise so that the relationship between them can be meaningfully discussed.

In the first instance, the basic "result" of a solution to a problem will be assumed to be a flux integrated quantity or more simply a response. We thus define:

$$R \equiv \int_{\bar{\xi}} \Sigma_R(\bar{\xi}) \; \phi(\bar{\xi}) \; d\bar{\xi} \equiv \left\langle \Sigma_R, \phi \right\rangle \tag{1}$$

Here, $\phi(\xi)$ is the angular flux solution of the Boltzmann transport equation, which in operator notation can be written as:

$$L\phi(\bar{\xi}) = S(\bar{\xi}) \tag{2}$$

$S(\bar{\xi})$ is the external source; L the Boltzmann operator; $\bar{\xi}$, represents a point in phase space and is a function of the conventional independent variables $\bar{r}$, $\bar{\Omega}$, and E; and $\Sigma_R(\bar{\xi})$, is the response function which relates the flux to the integrated response being studied. For convenience sake, integrals over all phase space $\bar{\xi}$ will be denoted by braces as is conventionally done to connote an inner product of two functions. The form of Eqs. (1) and (2) restricts the present discussion to problems with fixed sources. Further, but straightforward extensions of the theory are needed to develop a method for analyzing critical systems.

The second element of nomenclature requiring definition is the connotation of the term sensitivity. For our purposes the meaning of sensitivity will be derived from an explicit mathematical connection to be made between the result R and the cross-section data used to solve a specific problem.

This connection will be established using the adjoint flux $\phi*(\overline{\xi})$, which is a solution to the adjoint Boltzmann equation:

$$L*\phi*(\overline{\xi}) = S*(\overline{\xi}) \tag{3}$$

where, $S*(\overline{\xi})$ is the adjoint source and, $L*$ is the adjoint Boltzmann operator, which for a suitable choice of boundary conditions[16] satisfies the well-known inner product relationship:

$$\langle \phi, L*\phi* \rangle = \langle \phi*, L\phi \rangle \tag{4}$$

To connect the problem cross-section data included in the operator L to the final result, the adjoint source must be chosen to be the functional derivative of the result with respect to the flux,[2] which for this case gives,

$$S*(\overline{\xi}) = \Sigma_R(\overline{\xi}). \tag{5}$$

The sensitivity of the result R to cross section data can now be defined by the following inner product relationship involving the adjoint flux:

$$R_x \equiv \langle \phi*, L_x\phi \rangle \tag{6}$$

Here L_x is some operator in the subset $\{L_x\}$ of the Boltzmann operator L, whose definition and domain determine what input cross sections are being studied. The term $L_x\phi$ is then a source of radiation arising from the operation denoted by L_x, and R_x, therefore, represents an adjoint weighted production rate integrated over all phase space. R_x here will be referred to as the integrated sensitivity of the result to cross-section data included in L_x. Treating the integrand of the inner product in Eq. (7) as a density function describing the adjoint weighted production rate per unit volume in phase space, we can define $R_x(\overline{\xi})$, a differential sensitivity function as follows:

$$R_x(\overline{\xi}) = \phi*(\overline{\xi})L_x\phi(\overline{\xi}) \tag{7}$$

It will become clearer in the next section how $\bar{R}_x$ and $R_x(\bar{\xi})$ are related to the total result R and why Eqs. (7) and (8) will be referred to as the integrated and differential sensitivity of R to the data included in the operator L_x, respectively. Specifically, the interpretation of the adjoint flux as an importance function will be used to make the connection. Some mathematical interpretations of terms of the form of R_x, in particular their connection with the functionals in perturbation theory, and local derivatives of R with respect to cross section will also be discussed.

B. The Adjoint Flux as an Importance Function

The interpretation of the adjoint flux as a function describing the importance of particles in contributing to the final result is the under-lying physical basis of the general approach to sensitivity analysis. While many arguments can be used to justify such an interpretation,[16] for the purposes of this discussion a brief mathematical discussion of the adjoint flux Green's function offers clear justification for its use in this context.

Following a traditional course,[17] two alternative methods for computing the result R can be derived. The first involves a solution of the Boltzmann equation for $\phi(\bar{\xi})$ with subsequent calculation of the result R using Eq. (1) and a suitable response function $\Sigma_R(\bar{\xi})$. A second choice involves solving the adjoint Boltzmann equation for $\phi*(\bar{\xi})$ and then computing R from the following relationship:

$$R = \left\langle \phi*, S \right\rangle \tag{8}$$

Cross multiplication of Eqs. (2) and (5) by $\phi*(\bar{\xi})$ and $\phi(\bar{\xi})$ respectively, followed by an integration over all phase space $\bar{\xi}$, and subtraction of the two resulting equations establishes the fact that:

$$\left\langle \phi*, S \right\rangle = \left\langle \Sigma_R, \phi \right\rangle \tag{9}$$

From this well-known result, it is possible to construct the adjoint flux Green's function by simply letting the problem source $S(\overline{\xi})$ be a multi-dimensional Dirac delta function. That is, let:

$$S(\overline{\xi}) = \delta(\overline{\xi}-\overline{\xi}_o) \tag{10}$$

Substituting this expression into Eq. (9) and combining the result with Eq. (1), we get:

$$R = \int \Sigma_R(\overline{\xi})\phi(\overline{\xi}) \; d\overline{\xi} = \phi^*(\overline{\xi}_o) \tag{11}$$

Clearly $\phi^*(\overline{\xi}_o)$ quantitatively represents the contribution of particles born at the point $\overline{\xi}_o$ in phase space to the result R. For the case above where particles are born only at $\overline{\xi}_o$, $\phi(\overline{\xi}_o)$ is numerically equivalent to the total result R. For a distributed source $S(\overline{\xi})$, the linear nature of the Boltzmann operator allows $\phi^*(\overline{\xi})$ to be used as a Green's function to sum up the contribution of particles born at all point in phase space to arrive at the result R {i.e., R can be computed from Eq. (9)}.

This property of the adjoint flux establishes it physically as an importance function. That is, it is a quantitative measure of the importance of particles born at any point in phase space in contributing to the final result.

C. Cross-Section Sensitivity Analysis

Using the interpretation above, we can now answer the general analytic question of central importance in a sensitivity study--how do we measure the importance of an element of cross-section data in the solution of the Boltzmann equation? To make this determination, the result, as defined in Eq. (9), is rewritten in terms of the Boltzmann operator L defined in Eq. (2). That is:

$$R = \left\langle \phi^*,L\phi \right\rangle = \left\langle \phi^*(\overline{\xi}),L\phi(\overline{\xi}) \right\rangle \tag{12}$$

From the previously established interpretation of the adjoint flux as an importance function, it is now possible to make a quantitative assessment of the sensitivity of the result to the input cross-section data. Clearly,

$L\phi(\bar{\xi})$ is a production rate of radiation in phase space and $\phi*(\bar{\xi})L\phi(\bar{\xi})$ is its to contribution to the final result. If the Boltzmann operator is now broken down into a subset of operators $\{L_x\}$, the production rate associated with any sub-operator L_x can be identified separately as $L_x\phi(\bar{\xi})$. Since the Boltzmann equation is linear, the partial contribution to R of any inter-action contained in the definition of the operator L_x is given by $\phi*(\bar{\xi})L_x\phi(\bar{\xi})$. A differential or integral assessment of the sensitivity of the result R to data contained in L_x is therefore given by Eqs. (8) and (7), respectively. For cross-section sensitivity analysis, L_x will be a reaction-rate operator containing explicit reference to partial cross-section data from reaction type x as a function of energy. The energy region to be studied is understood to be determined by the domain of definition of L_x in phase space.

In dealing with specific subsets of L for cross section analysis in non-multiplying media, two types of terms are needed. One involves the operator for the loss of particles from a point in phase space as a result of particle interactions and the other, a double differential cross-section operator representing the scattering of particles into a point in phase space. Each involves the definition of a suitable sensitivity function through an appropriate choice of L_x and its domain of definition. The importance of collision losses can be determined in a straightforward manner with the following total cross-section sensitivity function:

$$R_{\Sigma_{x,\,LOSS}}(\bar{\xi}) \equiv \phi*(\bar{\xi})\ \Sigma_T(\bar{\xi})\ \phi(\bar{\xi}) \tag{13}$$

The total cross section is used to define the loss function, since any collision at $\bar{\xi}$ removes the particle from that point in phase space.

The scattering of particles into a point in phase space through specific reaction type x is determined by the double differential scattering cross section $\Sigma_x(E{\to}E',\bar{\Omega}{\to}\bar{\Omega}')$ for transfer from initial E and $\bar{\Omega}$ to final E' and $\bar{\Omega}'$. The increase in sensitivity at the final energy is thus given by a double differential sensitivity function:

$$R_{\Sigma_{x,GAIN}}(\bar{r},E',E,\bar{\Omega}',\bar{\Omega}) = \phi(\bar{r},E,\bar{\Omega})\ \Sigma_x(\bar{r},E{\to}E',\bar{\Omega}{\to}\bar{\Omega}')\ \phi*(\bar{r},E',\bar{\Omega}') \tag{14}$$

For specific analysis of cross-section behavior as a function of energy, both the loss and gain terms previously defined can be added to determine the total sensitivity of the result to a particular reaction cross section. Since cross-section data for transport calculations are usually specified in a number of homogeneous regions and the energy dependence of the data is of paramount concern, spatial and angular behavior can be eliminated by integration. We therefore define a sensitivity function for a particular reaction type by integrating the functions defined in Eqs. (13) and (14) over all angles and over a homogeneous spatial region, designated by $\bar{r}_o$. This gives:

$$R_{\Sigma_x}(E) = -R_{\Sigma_x,\text{LOSS}}(E) + R_{\Sigma_x,\text{GAIN}}(E) \tag{15}$$

Here, the first term represents the total sensitivity of $\Sigma_x(E)$ type collisions in removing a particle from energy E and the second term is the collective gain in sensitivity after emerging from such collisions at other energies and angles. The positive and negative signs in front of the terms reflect the effect of such losses or gains of sensitivity with respect to the result. The sum of these terms, $R_{\Sigma_{x(E)}}$, therefore, represents the energy dependent total sensitivity of the result R to reactions of type $\Sigma_x(E)$ at energy E.

A "sensitivity profile" can now be defined by normalizing the sensitivity density function given in Eq. (15). That is:

$$P_{\Sigma_x}(E) \equiv R_{\Sigma_x}(E)/R \tag{16}$$

The normalization allows $P_{\Sigma_x}(E)$ to reflect the fractional sensitivity of the result R to reactions of type $\Sigma_x(E)$ at energy E.

Writing out the explicit functional form of $P_{\Sigma_x}(E)$ for a particular reaction type, we get the following:

$$P_{\Sigma_x}(E) = \frac{\Sigma_x(E)}{R} \sum_{\ell} \left[\frac{2\ell + 1}{4\pi}\right] \int_{r_o} d\bar{r} \left[-\phi_\ell(\bar{r},E) \phi^*_\ell(\bar{r},E) \right.$$

$$\left. + \int_{E'} \phi_\ell(\bar{r},E) f^\ell_x(\bar{r},E \rightarrow E') \phi^*_\ell(r,E') dE' \right] \Big/ R \qquad (17)$$

Here, for convenience sake, the integral over solid angle $\bar{\Omega}$ in Eqs. (16) has been carried out by assuming azimuthal symmetry and expanding the flux and its adjoint in Legendre polynomials as opposed to associated Legendre polynomials needed for the general case. The angular moments are defined as follows:

$$\phi_\ell(\bar{r},E) = \int P_\ell(\mu) \phi(r,E,\bar{\Omega}) d\bar{\Omega} \qquad (18)$$

$$\phi^*_\ell(\bar{r},E) = \int P_\ell(\mu) \phi^*(\bar{r},E,\bar{\Omega}) d\bar{\Omega} \qquad (19)$$

$$\Sigma_x(E) f^\ell_x(\bar{r},E \rightarrow E') = \int P_\ell(\omega) \Sigma_x(\bar{r},E \rightarrow E',\bar{\Omega} \rightarrow \bar{\Omega}') d\omega$$

where $\mu = \bar{r} \cdot \bar{\Omega}$, $\omega = \bar{\Omega} \cdot \bar{\Omega}$, P_ℓ is a Legendre polynomial of order ℓ, and $f^\ell_x(\bar{r},E \rightarrow E')$ is the ℓth Legendre moment of the normalized secondary energy-angle distribution function for reaction type x at energy E.

This general form of a cross-section sensitivity function is particularly convenient from a computational point of view since spatial integrals of the Legendre moments of the flux appear explicitly in terms which are independent of the particular cross section $\Sigma_x(E)$ being studied. In fact, it is quite useful to define a special function for such terms in a homogeneous spatial region $\bar{r}_o$ in the form of a matrix. We thus define sensitivity matrix elements as:

$$M_\ell(E,E') \equiv \int_{\bar{r}_o} \phi_\ell(\bar{r},E) \phi^*_\ell(\bar{r},E') d\bar{r} \qquad (21)$$

In terms of this function, we can rewrite Eq. (17) in the same homogeneous zone as:

$$P_{\Sigma_x}(E) = \frac{\Sigma_x(E)}{R} \sum_{\ell} \left[\frac{2\ell + 1}{4\pi}\right] \left[- M_\ell(E,E) + \int_{E'} f_x^\ell(E \to E') M_\ell(E,E') \, dE' \right] \quad (22)$$

Eq. (22) is in a form which is easily applied to global cross-section sensitivity studies. Once forward and adjoint fluxes have been computed for a particular problem, the matrix $M_\ell(E',E)$ can be generated for use with any partial cross section. A sensitivity profile for an individual partial requires only a single integration of the cross section data and the sensitivity matrix elements over final transfer energy. With fairly straightforward computer algorithms, an analysis of all cross-section data used in solving a particular problem can be made without having to specify beforehand which cross sections were to be studied. Graphical display of $P_{\Sigma_x}(E)$ for all partial cross sections used in a given problem is a great aid in understanding particle transport,[2,8] and satisfies the need for a survey of the entire data field. The most important energy ranges for each partial cross-section set under study are clearly identified in such a plot by the maxima in the function.

D. Connections with Perturbation Theory

The other important aspect of the present approach to sensitivity analysis is its potential for predicting changes in R as a result of changes in the operators in $\{L_x\}$. To demonstrate this capability, the connection between a general sensitivity function $R(\bar{\xi})$ and the principles of perturbation theory will be examined.

The more formal mathematical implications of the definition introduced in Eq. (7) for discussing sensitivity are most easily developed by showing that such a mathematical form is a linear functional in perturbation theory. Starting from Eq. (13):

$$R = \langle \phi^*, L\phi \rangle \quad (23)$$

we can define a perturbed problem with a perturbed flux ϕ' and its adjoint $\phi*'$, a perturbed operator L' and its adjoint $L*'$, which satisfy the following equations:

$$L'\phi' = S \tag{24}$$

$$L*'\phi*' = S* \tag{25}$$

A result for the perturbed problem can then be found from the expression:

$$R' = \left\langle \phi*', L\phi \right\rangle \tag{26}$$

The relationship between the perturbed result, R', and the unperturbed result, R, can easily be established by letting the perturbation be defined

$$\phi' = \phi + \delta\phi \tag{27}$$

$$\phi*' = \phi* + \delta\phi* \tag{28}$$

$$L' = L + \delta L \tag{29}$$

$$L*' = L* + \delta L* \tag{30}$$

Expanding R' in terms of these quantities, together with some algebraic manipulations,[20] we can write the perturbed result simply as:

$$R' = R - \left\langle \phi*, \delta L\phi \right\rangle + \left\langle \delta\phi*, L'\delta\phi \right\rangle = R - \left\langle \phi*', \delta L\phi \right\rangle \tag{31}$$

From the standpoint of linear perturbation theory where second-order effects of the form of the third term on the right-hand side of Eq. (31) are ignored, we get:

$$R' - R = \delta R \stackrel{\sim}{=} - \left\langle \phi*, \delta L\phi \right\rangle \tag{32}$$

It is this relationship that clearly defines the connection between the analyti ' and predictive aspects of the definition offered in Eq. (8) for discussing sensitivity. If L_x in that equation is defined as the perturbed operator δL, then we can formally write R_x for this case as:

$$R_x \equiv R_{\delta L} = \left\langle \phi*, \delta L\phi \right\rangle \stackrel{\sim}{=} - \delta R \tag{33}$$

The integrated sensitivity function as applied to answering the second fundamental sensitivity question—how will a calculated result change as a result of changes in the input data? -- can be interpreted as the first-order change in the result arising from the data change specified in δL.

With this relationship formally established, Eqs. (13), (14), and (22) defined in the previous section can be applied to perturbed problems to predict changes in the result. For such applications, $\delta\Sigma_x(E)$ can be inserted into these expressions in place of $\Sigma_x(E)$. This procedure is particularly powerful because the sensitivity of the result to changes in an operator can be determined as a function of phase space. For instance, energy-dependent cross-section uncertainti. , represented by $\delta\Sigma_x(E)$, can be incorporated into the definition of the sensitivity profile $P_{\Sigma_x}(E)$ given in Eq. (22) such that a graphical display of a first-order approximation to $\delta R_{\Sigma_x}(E)/R$ can be presented for a series of spatial zones as a function of energy. An energy-dependent assessment of the effect of these cross-section uncertainties on the final result is immediately available from such a plot. This function is as useful in determining which cross-section uncertainties are important in a given problem, as is the expression given in Eq. (22) for determining which cross sections are important. It also points out those cross sections which are most responsible for uncertainties in transport calculations and should serve as a guide to cross-section measurers and evaluators.

E. Interpretation in Terms of Partial Derivatives

In addition to its direct connection with perturbation theory functionals, the cross-sections sensitivity function can be interpretated physically as a differential rate of change of the result R with respect to the cross sections in L_x. This interpretation can be illustrated for a general class of operators (which include cross-section operators) of the following form:

$$L\,\phi = \sum_i L_{\alpha_i}\,\phi = \sum_i \alpha_i(\zeta)\,L_i\phi \tag{34}$$

where the α_i's are parameters whose sensitivity one is interested in studying, and the L_i's are operators independent of the α_i's. Here in particular α_i is an energy-dependent cross section $\Sigma_x(E)$.

Using perturbation theory, we can develop an expression for δR in terms of such an operator by starting with Eq. (31). Thus, we introduce a perturbation in a specific region of phase space $\overline{\Delta\xi}$ with a δL defined as follows:

$$\delta L \equiv \begin{cases} \delta\alpha_i(\overline{\xi})\ L_i\phi & \overline{\xi} - \dfrac{\overline{\Delta\xi}}{2} \le \overline{\xi} \le \overline{\xi} + \dfrac{\overline{\Delta\xi}}{2} \\[2mm] 0 & \text{Elsewhere} \end{cases} \tag{35}$$

Here, $\overline{\xi} \pm (\overline{\Delta\xi}/2)$ is understood to be of the form $(x \pm \Delta x/2,\ y \pm \Delta y/2,$ etc.). The perturbation in the result will then be given by:

$$- \delta R = \int_{\overline{\xi}-(\overline{\Delta\xi}/2)}^{\overline{\xi}+(\overline{\Delta\xi}/2)} \phi*'\delta L\phi\ d\overline{\xi} \tag{36}$$

If we now assume that $\delta\alpha_i/\alpha_i$ is a constant in the perturbed region, we can rewrite Eq. (36), making use of the definition of the perturbation given in Eq. (35), to get:

$$- \delta R = \frac{\delta\alpha_i}{\alpha_i} \int_{\overline{\xi}-(\overline{\Delta\xi}/2)}^{\overline{\xi}+(\overline{\Delta\xi}/2)} \phi*'\alpha_i L_i \phi\, d\overline{\xi} \tag{37}$$

This can be rewritten as:

$$\frac{- \delta R}{(\delta\alpha_i/\alpha_i)\ \overline{\Delta\xi}} = \frac{\displaystyle\int_{\overline{\xi}-(\overline{\Delta\xi}/2)}^{\overline{\xi}+(\overline{\Delta\xi}/2)} \phi*'L_{\alpha_i}\phi\, d\overline{\xi}}{\overline{\Delta\xi}} \tag{38}$$

If the perturbed region contains no source singularities then $\phi*L_{\alpha_i}\phi$ will be a continuous, bounded function, and we can let $\overline{\Delta\xi}$ approach a differential region in phase space and $\delta\alpha_i/\alpha_i$ approach zero. In this limit we get:

$$\phi*' \to \phi* \tag{39}$$

$$\overline{\Delta\xi} \to \overline{\partial\xi} \tag{40}$$

$$\frac{\partial R}{(\delta\alpha_i/\alpha_i)} \to \frac{\partial R}{\partial(\ln\alpha_i)} \tag{41}$$

and therefore:

$$\frac{-\partial R}{\partial(\ln\alpha_i)\ \overline{\partial\xi}} = \phi^* L_{\alpha_i} \phi = R_{\alpha_i}(\overline{\xi}) \tag{42}$$

Thus, in this instance the differential sensitivity function, $R_{\alpha_i}(\overline{\xi})$, is related to the local rate of change of the result with respect to a logarithmic change in the sensitivity parameter α_i. The sensitivity profile which is given by

$$P_{\alpha_i}(\overline{\xi}) = R_{\alpha_i}(\overline{\xi})/R = \frac{-\partial R/R}{\partial\alpha_i/\alpha_i\ \partial\overline{\xi}} \tag{43}$$

then represents a differential density function for the percent change in R per percent change in the sensitivity parameter α_i per unit volume in phase space. This interpretation will be used extensively in the discussion of the air transport calculation which follows.

It should be noted at this point, that in actual implementation of the techniques outlined in this section, multigroup discrete-ordinates transport methods are used extensively. For this reason, the basic formulas given in Eqs. (17), (33), and (43) must be replaced by their equivalent discrete-ordinates multigroup expression. In the case of the sensitivity profile, the point-energy density function $P_{\Sigma_x}(E)$ given in Eq. (17) is converted into a point-lethargy function $P_{\Sigma_x}(u)$ and written in multigroup for m:

$$P_{\Sigma_x}(u) = \lim_{\Delta u_g \to 0}\frac{\displaystyle\int_{u_g}^{u_{g+1}} P_{\Sigma_x}(u)\ du}{\displaystyle\int_{u_g}^{u_{g+1}} du} = \frac{P_{\Sigma_{x,g}}}{\Delta u_g} \tag{44}$$

where

$$P_{\Sigma_{x\to g}} = \left[-\sum_j\sum_k \phi^*_{j,k,g}\ \phi_{j,k,g}\ \Sigma_{x,j,g}\ \Delta V_j\ \Delta\Omega_k \right.$$
$$\left. +\sum_j\sum_\ell\sum_{g'} \phi^{*\ell}_{j,g'}\ ^{*\ell}_{j,g}\ \Sigma^\ell_{x,j,g\to g'}\ \Delta V_j\right]\Big/ R \tag{45}$$

The multigroup discrete ordinate notation is that used in Ref. 20 (j=space, k=angle, ℓ=Legendre moment, g=group) for the equations solved by ANISN transport code which was used to obtain the fluxes in the above equations. Note the 2ℓ+1 and 4π factors from Eq. (17) are absorbed in the definition of the flux and transfer cross sections for ANISN.

A similar expression for predictive applications can be derived from Eq. (33) as follows:

$$\frac{\delta R}{R} = \int \left(\frac{\partial R/R}{\partial \Sigma_x/\Sigma_x}\right) \frac{\partial \Sigma_x}{\Sigma_x} \, du = \int_u P_{\Sigma_x} (u) \frac{\delta \Sigma_x}{\Sigma_x} \, du$$

$$\cong \sum_g P_{\Sigma_{x,g}} \left(\frac{\delta \Sigma_x}{\Sigma_x}\right)_g \tag{46}$$

where $P_{\Sigma_{x,g}}$ is given in Eq. (45) and $(\delta \Sigma_x/\Sigma_x)_g$ is the fractional cross section change of cross section type Σ_x in Group g.

III. CALCULATIONS AND RESULTS

A. Problem Description

To illustrate how the theoretical methods discussed in the previous section can be applied in practical situations, an air transport problem will be analyzed using both the analytic and predictive aspects of sensitivity theory. The air transport problem considered here is the determination of total (neutron and gamma ray) tissue dose in air at 2000 meters from an unclassified thermonuclear source.[18] Forward and adjoint calculations were made using the one-dimensional discrete ordinates code ANISN[19] while the cross-section sensitivity analysis was performed using the SWANLAKE[20] code. The ANISN calculations were run in spherical geometry with an S_{16} Gauss-Legendre angular quadrature set and a P_3 Legendre expansion of the scattering kernel. The cross sections used in the calculation were ENDF/B-III Mat 1133, Mod 3,* for ^{14}N and Mat 1134, Mod 1,* for ^{16}O. The ENDF/B-III cross sections were processed into a 101-33 coupled neutron-gamma ray energy group structure which included neutron groups tailored to fit important features in the total neutron air cross section and gamma-ray groups bracketing important

---

*The ENDF/B-III cross-section sets used here correspond to Defense Nuclear Agency Mat 4133 (^{14}N) and Mat 4134 (^{16}O).

gamma-ray production lines. The number densities in atoms per barn-cm used were 3.664×10^{-5} for ^{14}N and 9.74×10^{-6} for ^{16}O, and the calculations were extended to 3000 meters of air to allow for reflection. The tissue dose was determined with the Snyder-Neufeld[21] response function for neutrons and the Henderson[22] response function for gamma rays. The total tissue dose at 2000M from a point isotropic neutron source of 1 n/sec was determined to be 2.40×10^{-23} rads/sec by an ANISN forward calculation, with a neutron tissue dose of 1.75×10^{-23} rads/sec ($\sim 73\%$ of total dose), and a gamma tissue dose of 0.65×10^{-23} rads/sec ($\sim 27\%$ of total dose). The ANISN adjoint calculation used for the sensitivity analysis gave a total tissue dose of 2.45×10^{-23} rads/sec, showing agreement within $\sim 2\%$ of the result obtained in the forward calculation.

The energy group structure employed for the neutron cross sections is presented in Appendix A along with the unclassified thermonuclear source and the tissue dose response function employed for each group. Appendix A also presents the energy group structure for the gamma ray cross sections and the tissue dose response function for each group. The neutron source and the response functions for neutrons and gamma rays are presented graphically in Figs. (1) through (3), respectively. It should be noted that both the neutron and gamma-ray tissue dose response functions are predominantly responsive to high energy radiation, while the source distribution is dominated by neutrons in the 0.01 MeV and 10 MeV ranges. A preliminary investigation[23] indicated that this thermonuclear source spans the important energy ranges of both 14 MeV and fission sources, and so is somewhat representative of a general source for coupled neutron and gamma-ray air transport problems. However, direct extension of sensitivity results for the thermonuclear case to calculations for other sources is a difficult task and is not a recommended procedure.

B. Sensitivity Profiles for Air Cross Sections

To illustrate the analytic aspect of a sensitivity analysis, a series of sensitivity profiles for several partial cross sections of nitrogen and oxygen can now be presented. The sensitivity profile (a plot of sensitivity per unit lethargy vs energy) as described before is intended

Fig. 1. Unclassified Thermonuclear Source[18] Per Unit Lethargy.
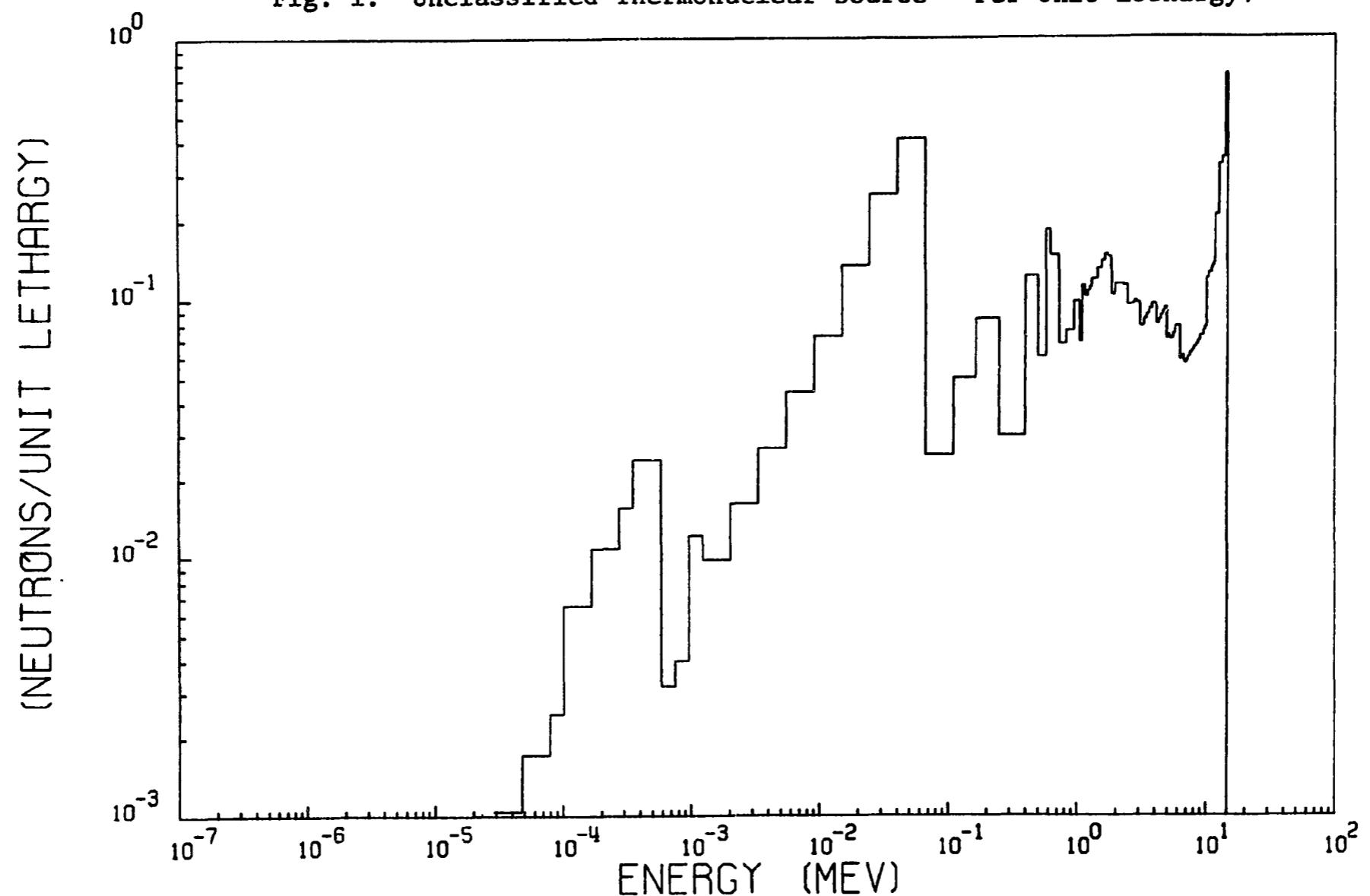
Fig. 2. Snyder-Neufeld Neutron Tissue Dose[21] Response Function.
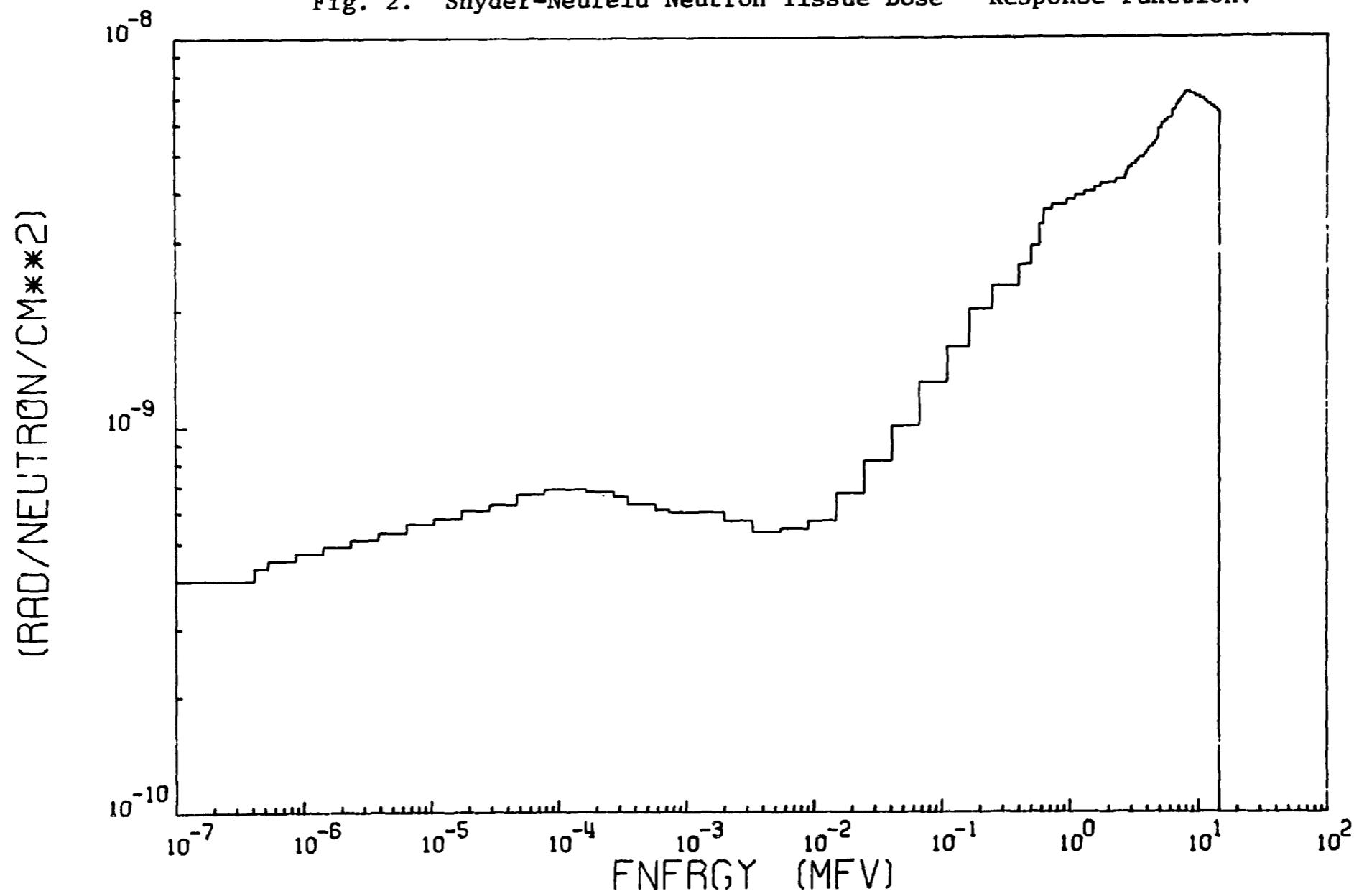
Fig. 3. Henderson Gamma Tissue Dose[22] Response Function.
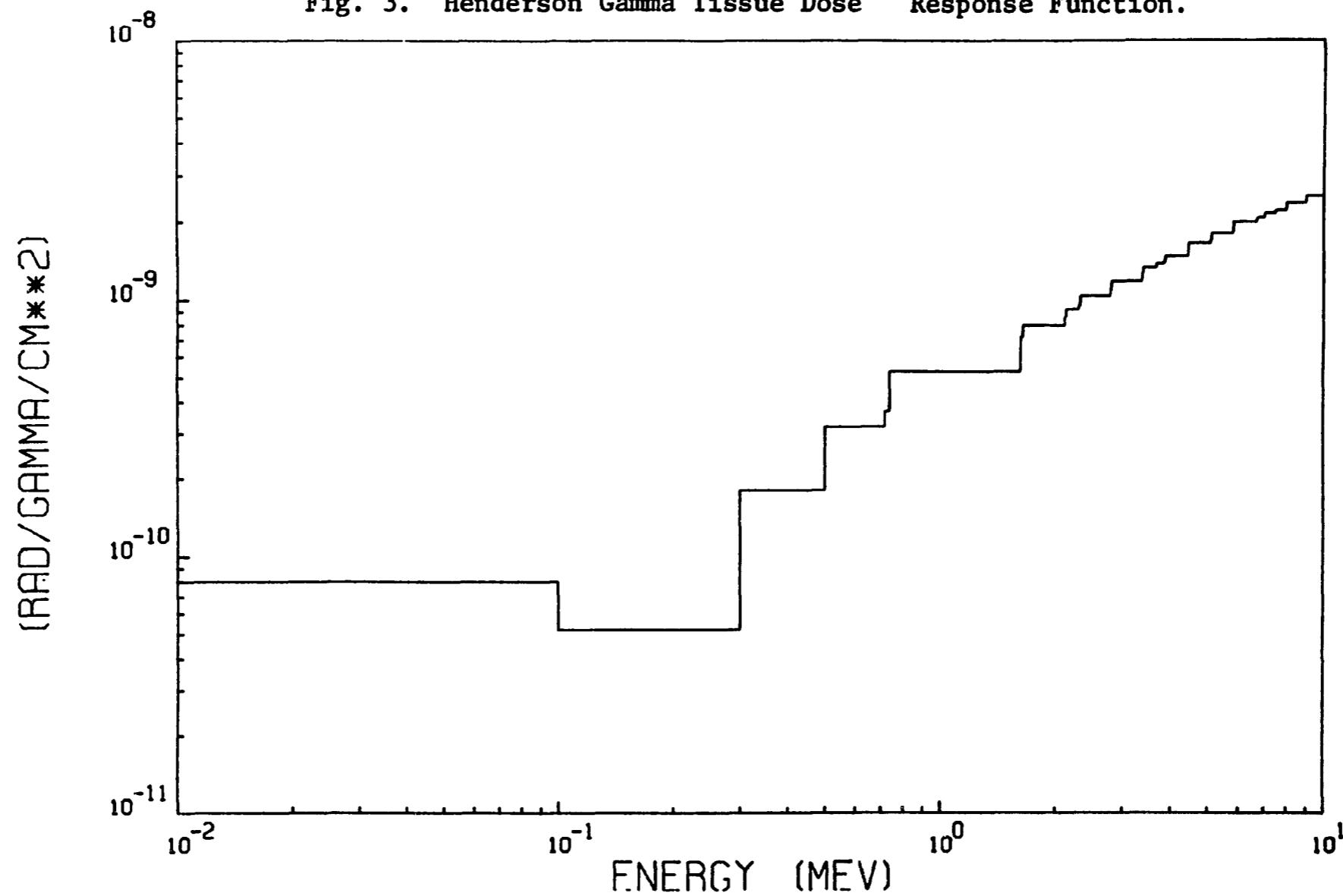
to provide a visual display of the importance of a given cross section in a specific calculation as a function of energy. It also represents quantitatively the differential rate of change of the result (tissue dose) with respect to changes in the cross section as a function of energy. The histogram bins used in all the figures to follow represent the energy group structure utilized in the calculation. Solid lines will be used to indicate negative sensitivity (energy regions in which increases in cross section cause decreases in the response or tissue dose for this case) and dashed lines used to indicate positive sensitivity (regions where increases in cross section cause increases in the response). In general, values greater than 1.0 on a sensitivity profile indicate regions of high sensitivity. Sensitivity profiles can and are normally obtained for each of the individual reaction cross sections in the ENDF/B listings for every nuclide appearing in the calculation which is being analyzed. This paper will deal only the more interesting and important sensitivity profiles for this problem, but a complete set is presented in Appendix B. Although neutron energy groups extended down to 10^{-7} MeV in the calculation, the sensitivity profiles stop at 10^{-2} MeV since the lower energy neutrons showed relatively little importance for the calculation analyzed here.

Figure 4 shows a typical sensitivity profile, that for the total of all neutron cross sections in air which were used in this calculation. Both the neutron and gamma tissue doses are influenced by the neutron cross sections since they are responsible for the neutron transport process as well as secondary gamma-ray production. However, calculations have been made which indicate that for this problem the sensitivity of the total dose to the neutron cross sections are largely (about 95%) due to their effect on the neutron tissue dose. The term total collision profile will be used to refer to a profile which the sum of all the individual cross sections for a given isotope, so that Σ_{T_x} appearing in the description of a profile refers to cross section for reaction type x and $\Sigma_{T_{COLL}}$ refers to the total cross section (summed over all x).

Fig. 4. Sensitivity of Total Tissue Dose to Air (N_2+O_2) Neutron Total Cross Section.
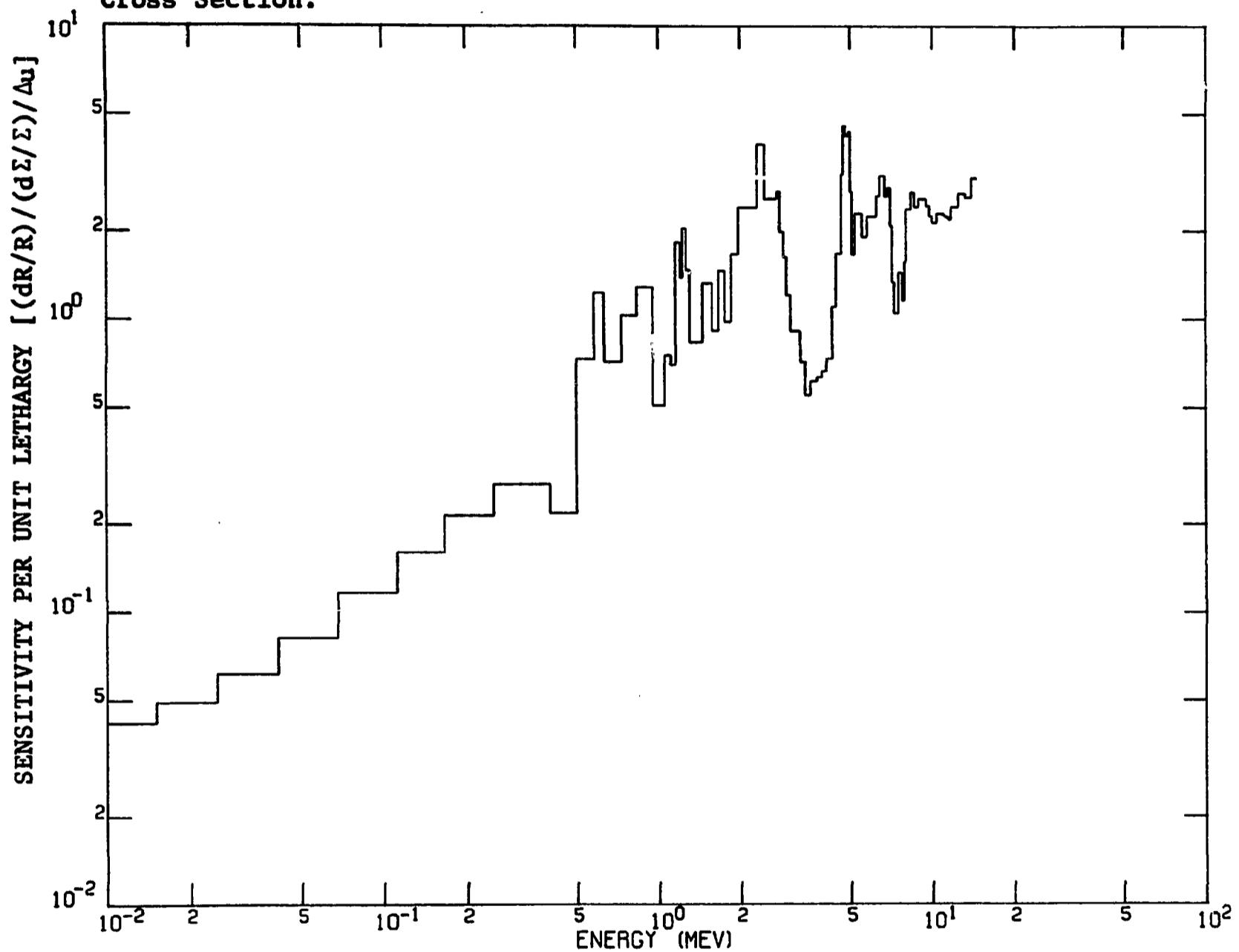
The illustrative profile shows that the energy range of primary importance for neutron collision cross sections for this problem extends from 14.5 MeV to about 2 MeV, with a range of secondary but still significant importance extending down to about 0.5 MeV. Approximately 88% of the total sensitivity to neutron cross sections (sensitivity to neutron collision cross sections, summed over all energies) is due to neutrons with energies above 0.5 MeV. This effect may at least partially be ascribed to the Snyder-Neufeld response function shown in Fig. (2) which decreases by a factor of 2 from 14.5 MeV to 0.6 MeV, then decreases at a much faster rate, dropping by a factor of 6 from 0.6 MeV to 0.01 MeV. The high energy bias of the source as illustrated in Fig. (1) also contributes to the high-energy dominance of the sensitivity profile in Fig. (4). In particular, the high sensitivity to neutron collision cross sections above 8 MeV is indicative of the importance of the high energy portion of the source for many deep penetration problems.[2,20] The structure in the profile from about 10 MeV to about 2 MeV is primarily due to variations in the total cross section of air. Peaks in the sensitivity profile for deep penetration transport problems, such as this one in air, frequently correspond to local minima in Σ_{T} and valleys in the sensitivity profile frequently correspond to energy regions where Σ_{T} is relatively high. For example, the two largest sensitivity peaks in Fig. (4) can be readily identified with the nitrogen Σ_{T} minimum at about 4.85 MeV and with the oxygen Σ_{T} minimum at about 2.37 MeV, respectively. The broad, deep valley in the sensitivity profile around 4.0 MeV corresponds to a fairly high Σ_{T} area for both nitrogen and oxygen from about 3.2 MeV to about 4.6 MeV, and another valley appears in the 7.2 to 8 MeV energy range, again corresponding to a fairly high Σ_{T} area.

Figure (5) presents the tissue dose sensitivity to the gamma-ray collision cross sections for air. Only the gamma dose in this case is affected by the gamma transport cross sections. Below 6 MeV the sensitivity profile generally follows the gamma dose response function shown in Fig. (3), which decreases with decreasing energies. The profile also generally decreases from 6 MeV up to 10 MeV, presumably because of the lower production rate of high energy gammas for this problem. This profile is smoother in overall shape than the neutron cross section profile in Fig. (4)

Fig. 5. Sensitivity of Total Tissue Dose to Air (N_2+O_2) Gamma Total Cross Section.
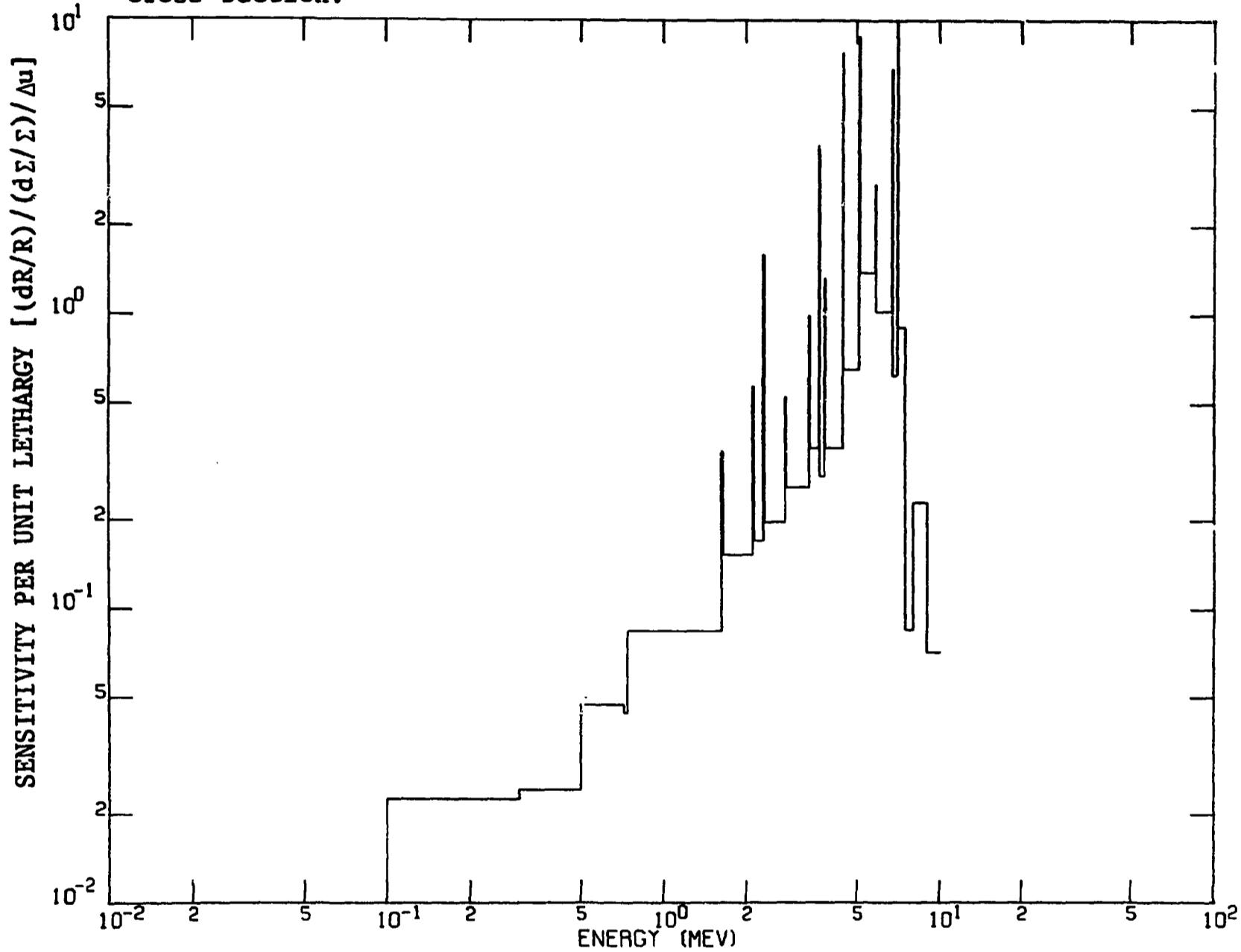
because of the lack of structure in Σ_T for the gamma cross sections. The structure which does appear in the profile is primarily due to the prominent discrete gamma-ray production lines. The spikes on Fig. (5) represent gamma groups with a 0.02 MeV width centered about specific production lines. The profile values were especially high for gamma groups representing gamma-ray production lines at 7.03 MeV, 6.72 MeV, 5.1 MeV, 4.44 MeV, 3.68 MeV, and 2.3 MeV, respectively. It is interesting to note that the gammas at 2.3 MeV, 5.1 MeV, and 7.03 MeV are associated with strong nitrogen inelastic excitation levels 1, 4, and 9, respectively, and the 6.7 MeV gamma corresponds to the third excitation level for the nitrogen (n,p) reaction.

C. Summary of Sensitivity Results

Calculations were made of the sensitivity of the total tissue dose to each specific reaction cross section for nitrogen and oxygen in the ENDF/B-III listings. Table I summarizes the results of these calculations by listing the integral sensitivities of the result to particular partial cross sections. The values given represent the percent change in dose resulting from a 1% increase at all energies in that specific cross section (equivalent to a 1% increase in the air density so that $(\delta \Sigma_x/\Sigma_x)_g$ in Eq. (46) is 0.01). The tissue dose is primarily sensitive to nitrogen neutron cross sections, as expected since the total tissue dose was about 75% neutron tissue dose, and the nitrogen to oxygen atomic ratio was $\sim$ 4 to 1. The neutron collision cross sections for nitrogen and oxygen are composed of the elastic, inelastic, and various absorption reaction cross sections, and the sensitivity to neutron collision cross section will similarly be composed of the sensitivities to the elastic, inelastic, and absorption reaction cross sections. The sensitivity to elastic cross sections comprises the greatest part of the sensitivity to neutron cross sections as is expected, since the elastic is normally the dominant reaction cross section, especially at lower energies. It should be noted, however, that the elastic cross section is relatively less important for nitrogen (a sensitivity of -3.17 out of -5.25) than for oxygen (-0.94 out of -1.16) for this problem. The sensitivity to inelastic cross sections is fairly high, but not as great as the

Table I. Sensitivity of the Total Tissue Dose
to the Indicated Nitrogen and Oxygen Cross Sections

Reaction	Sensitivity (Relative Importance)		
	N_2	O_2	Air (Total)
Σ_{COLL} (N + γ)	-6.08	-1.42	-7.50
Σ_{COLL} (N)	-5.25	-1.16	-6.41
Σ_{COLL} (γ)	-0.83	-0.26	-1.09
Σ_{EL}	-3.17	-0.94	-4.11
Σ_{INEL}	-0.55	0.09	-0.64
Σ_{ABSN}	-1.53	-0.13	-1.66
$\Sigma_{(N,\gamma)}$	+0.12	0.00	+0.12
$\Sigma_{(N,P)}$	-0.45	-0.01	-0.46
$\Sigma_{(N,D)}$	-0.10	0.00	-0.10
$\Sigma_{(N,T)}$	-0.08		-0.08
$\Sigma_{(N,P)} + \Sigma_{(N,D)} + \Sigma_{(N,T)}$	-0.63	-0.01	-0.64
$\Sigma_{(N,\alpha)}$	-1.00	-0.12	
$\Sigma_{(N,2\alpha)}$	-0.02		-0.02
$\Sigma_{(N,2N')}$	0.00		0.00

sensitivity to neutron absorption cross sections, especially for nitrogen. The absorption reactions are those in which no secondary neutrons appear as a product. Although the neutron and absorption reactions for air do produce secondary gamma rays, except for the nitrogen (n, 2α) and the oxygen (n,d) reactions, for this problem the sensitivities to these neutron cross sections are dominated by their influence on the neutron tissue dose, as indicated earlier. The neutron absorption cross sections are composed of the various reaction cross sections listed below the title Σ_{ABSN} in Table I, and·the sensitivities to the absorption cross sections are likewise the sum of the sensitivities to the reaction cross sections listed below absorption. The subtotal created for the nitrogen (n,p), ⟨n,d), and (n,t) reactions is intended for use in conjunction with the error file presented in Section IV. The tissue dose sensitivity to nitrogen absorption cross sections is primarily due to cross sections for the nitrogen (n,α) reaction, with the sensitivity to the nitrogen (n,p) reaction cross sections also fairly high. The positive sensitivity given to the nitrogen (n,γ) cross sections indicates that an increase in the cross sections would cause an increase in the total tissue dose. This results from replacing a low-energy neutron which has a low probability of contributing to the tissue dose with a high-energy gamma ray which has a high probability of contributing to the dose.

D. Sensitivity Profiles for Selected Cross Sections

The sensitivity profiles presented here are for the cross sections which are most important for this problem, as indicated by Table I. The important features for these profiles are discussed and probable explanations for these features are given. In particular, an attempt is made to identify the cross sections primarily responsible for the major features in the sensitivity profile for air neutron collision cross sections given in Fig. (4).

Figure 6 presents the profile for nitrogen neutron collision cross sections, which is generally very similar to the air profile in Fig. (4) although there is some divergence around 1 MeV. The features of Fig. (6)

Fig. 6. Sensitivity of Total Tissue Dose to Nitrogen Neutron Total
Cross Section.

are caused by the combined effects of-all the nitrogen partial cross
sections.

Figure 7 gives the sensitivity profile for the nitrogen elastic
cross sections. Sensitivity to the elastic cross sections clearly dominates
the sensitivity to the nitrogen collision cross sections below about 2.5
MeV but falls off sharply between 3 MeV and 4.5 MeV, is fairly significant
from 4.5 MeV to about 7.2 MeV then decreases in importance at higher
energies, especially about 10 MeV where the elastic contribution to Fig.
(6) is very small. The sensitivity is positive for three regions in Fig.
(7), those from 4.3 MeV to 4.1 MeV, from 4.1 MeV to 3.95 MeV, and from
3.6 MeV to 3.45 MeV. A dotted line on the high energy side of a histo-
gram bar in Fig. (7) indicates that an increase in the nitrogen elastic
cross section in that group would cause an increase in the tissue dose.
This positive sensitivity occurs because the cross section for the
nitrogen (n,α) reaction peaks in those groups. The nitrogen (n,α) reaction
produces few gammas and acts primarily as a particle sink, resulting in
a highly negative sensitivity. Elastic scattering of neutrons out of these
groups into groups where absorption is less likely therefore increases
their probability of contributing to the tissue dose, even though an
energy degradation occurs.

The sensitivity profile for the nitrogen inelastic cross sections
is given in Fig. (8). The inelastic contribution to Fig. (6) is not too
large, and is primarily important above 10 MeV. The inelastic sensitivity
profile is entirely negative, indicating that the effect of a large energy
downscatter on the neutron dose overshadows the effect of secondary gamma
ray production on the gamma tissue dose for this problem.

Figure (9) presents the sensitivity profile for the nitrogen absorp-
tion reactions which is fairly significant above 2 MeV and is especially
important above 10 MeV, in the 5 MeV nitrogen minimum, and in the 2.37
MeV oxygen minimum. These minima in the total cross section are due
primarily to minima in the elastic cross sections, and serve as "windows"
for deep neutron penetration in that the flux tends to build up in them.

ORNL-DWG 72-12701

Fig. 7. Sensitivity of Total Tissue Dose to Nitrogen Neutron Elastic Cross Section.

are caused by the combined effects of-all the nitrogen partial cross sections.

Figure 7 gives the sensitivity profile for the nitrogen elastic cross sections. Sensitivity to the elastic cross sections clearly dominates the sensitivity to the nitrogen collision cross sections below about 2.5 MeV but falls off sharply between 3 MeV and 4.5 MeV, is fairly significant from 4.5 MeV to about 7.2 MeV then decreases in importance at higher energies, especially about 10 MeV where the elastic contribution to Fig. (6) is very small. The sensitivity is positive for three regions in Fig. (7), those from 4.3 MeV to 4.1 MeV, from 4.1 MeV to 3.95 MeV, and from 3.6 MeV to 3.45 MeV. A dotted line on the high energy side of a histogram bar in Fig. (7) indicates that an increase in the nitrogen elastic cross section in that group would cause an increase in the tissue dose. This positive sensitivity occurs because the cross section for the nitrogen (n,α) reaction peaks in those groups. The nitrogen (n,α) reaction produces few gammas and acts primarily as a particle sink, resulting in a highly negative sensitivity. Elastic scattering of neutrons out of these groups into groups where absorption is less likely therefore increases their probability of contributing to the tissue dose, even though an energy degradation occurs.

The sensitivity profile for the nitrogen inelastic cross sections is given in Fig. (8). The inelastic contribution to Fig. (6) is not too large, and is primarily important above 10 MeV. The inelastic sensitivity profile is entirely negative, indicating that the effect of a large energy downscatter on the neutron dose overshadows the effect of secondary gamma ray production on the gamma tissue dose for this problem.

Figure (9) presents the sensitivity profile for the nitrogen absorption reactions which is fairly significant above 2 MeV and is especially important above 10 MeV, in the 5 MeV nitrogen minimum, and in the 2.37 MeV oxygen minimum. These minima in the total cross section are due primarily to minima in the elastic cross sections, and serve as "windows" for deep neutron penetration in that the flux tends to build up in them.

ORNL-DWG 72-12701

Fig. 7. Sensitivity of Total Tissue Dose to Nitrogen Neutron Elastic Cross Section.

Fig. 8. Sensitivity of Total Tissue Dose to Nitrogen Neutron Inelastic Cross Section.
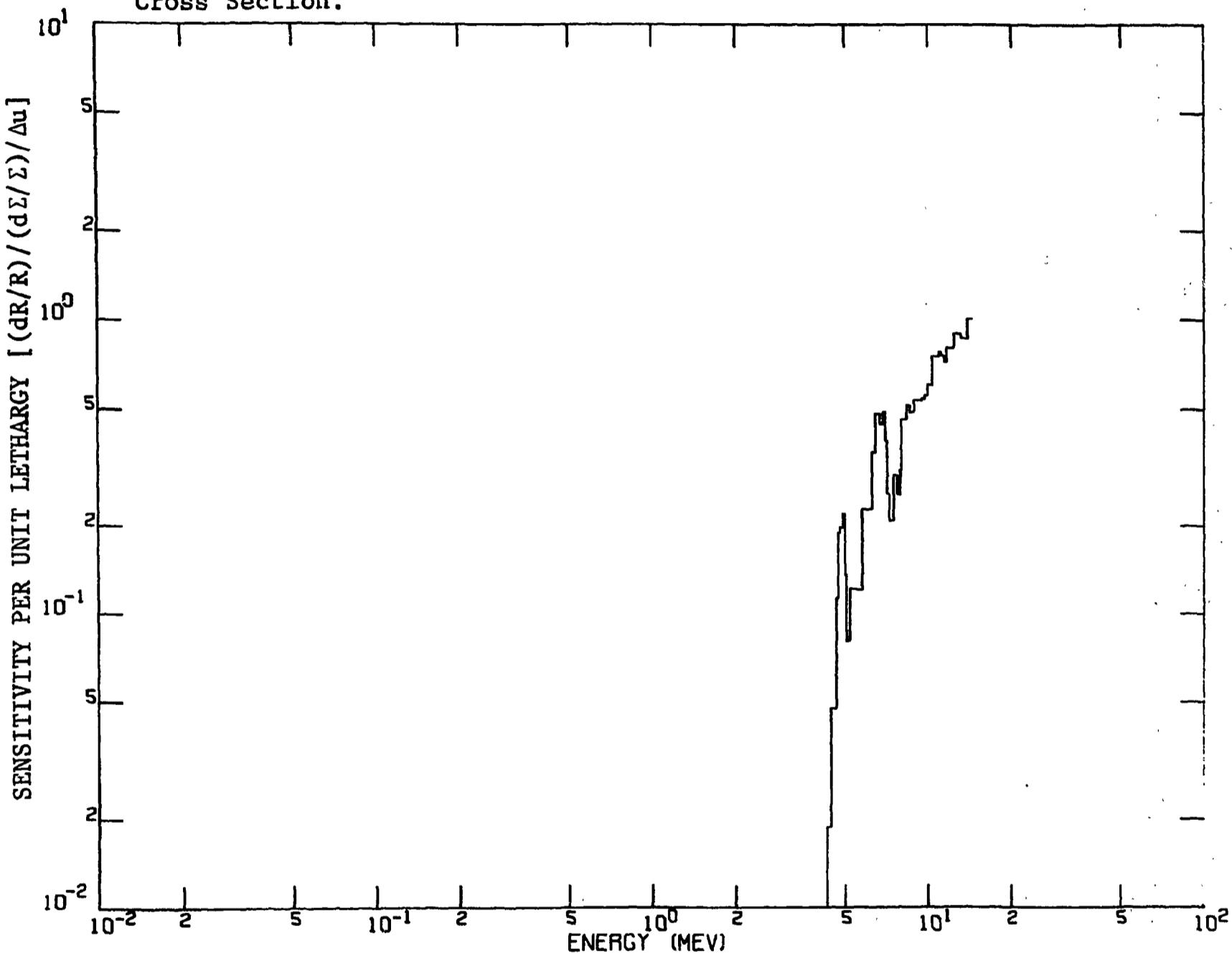
ORNL-DWG 72-12516

Fig. 9. Sensitivity of Total Tissue Dose to Nitrogen Neutron Absorption Cross Section.
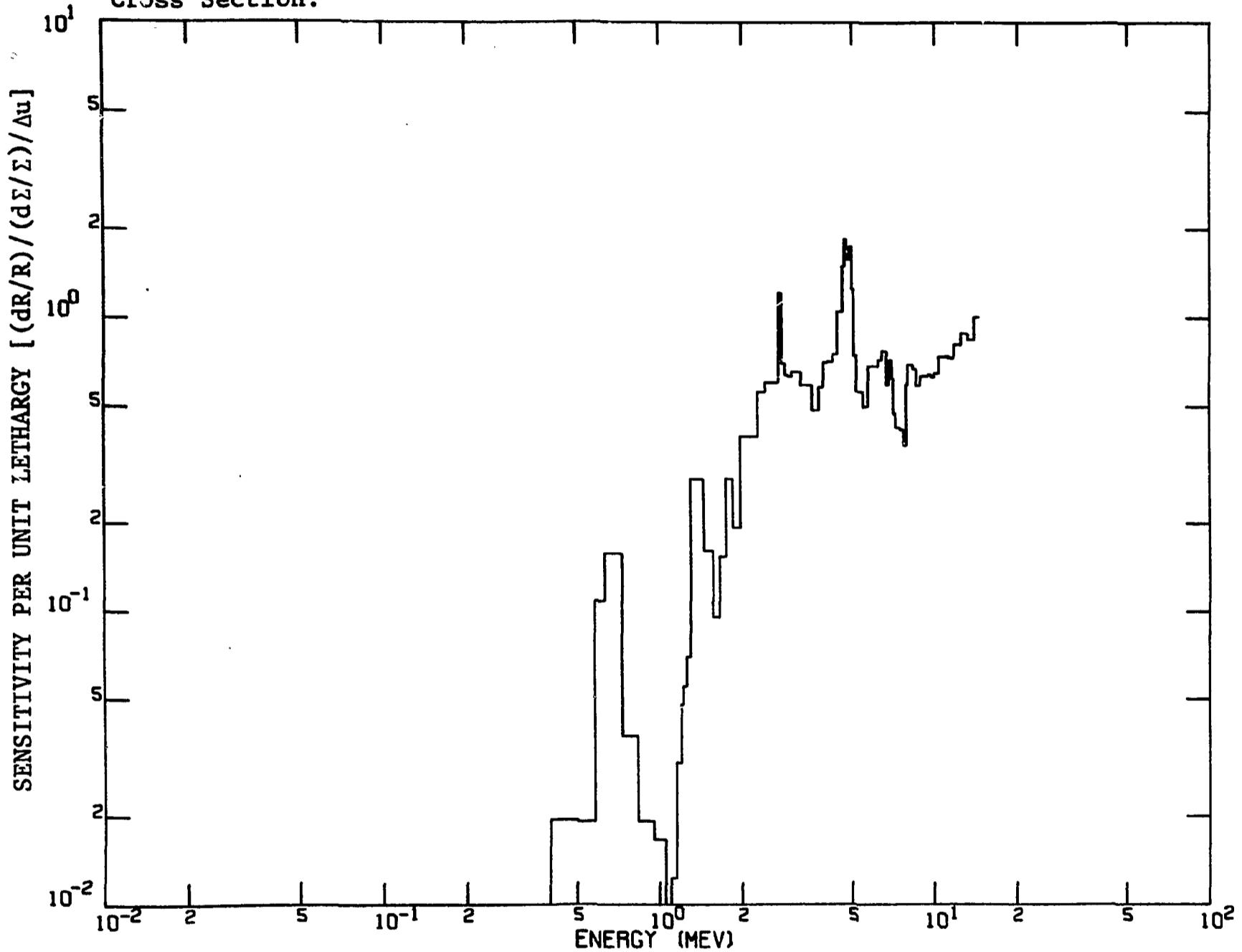
Absorption reactions in these minima have a high negative sensitivity since they remove neutrons which had a high probability of contribution to the dose.

Figures (10) and (11) give the sensitivity profiles for the nitrogen (n,α) and for the combined nitrogen (n,p), (n,d) and (n,t) reaction cross sections, respectively. Together these two figures account for most of the effects noted in Fig. (9). Specifically, Fig. (10) shows that the nitrogen (n,α) reaction cross sections account for most of the sensitivity to nitrogen absorption cross sections from 2 MeV to about 10 MeV, especially in the 5 MeV nitrogen minimum. Above 10 MeV the nitrogen (n,α) effect is less significant. Figure (11) shows a high sensitivity in the 2.37 MeV oxygen minimum and has a higher sensitivity above 10 MeV than does Fig. (10). Detailed calculations show that the nitrogen (n,p) reaction cross sections are responsible for the sensitivity "spike" at the oxygen minimum and for the structure at lower energies, while the nitrogen (n,d) cross sections are primarily responsible for the fairly high sensitivity above 10 MeV. The nitrogen (n,t) cross sections make a smaller contribution to the sensitivity profile above 10 MeV and a slight contribution in the vicinity of the 5 MeV nitrogen minimum.

The sensitivity profile for oxygen collision cross sections is presented in Fig. (12). Only two energy regions here make a significant contribution to the air collision cross section sensitivity profile in Fig. (4). The primary area of importance of oxygen cross sections is in the 1.5 MeV to 0.4 MeV range, where the oxygen collision cross section has several peaks and the overall sensitivity is low. The oxygen cross sections also make some contribution to the high sensitivity at the 5 MeV nitrogen minimum in Fig. (4), especially the single-group sensitivity "spike" which arises from a small peak in the oxygen collision cross which occurs in the middle of the nitrogen minimum. The sensitivity to the oxygen collision cross sections goes positive around 3.5 MeV where the nitrogen (n,α) cross section has a peak. This phenomenon was also observed in the nitrogen elastic cross section sensitivity profile in Fig. (7), and indicates that the elastic cross section is dominant over oxygen absorption reactions in this region.

ORNL-DWG 72-12520

Fig. 10.   Sensitivity of Total Tissue Dose to Nitrogen (N,α) Cross Section.
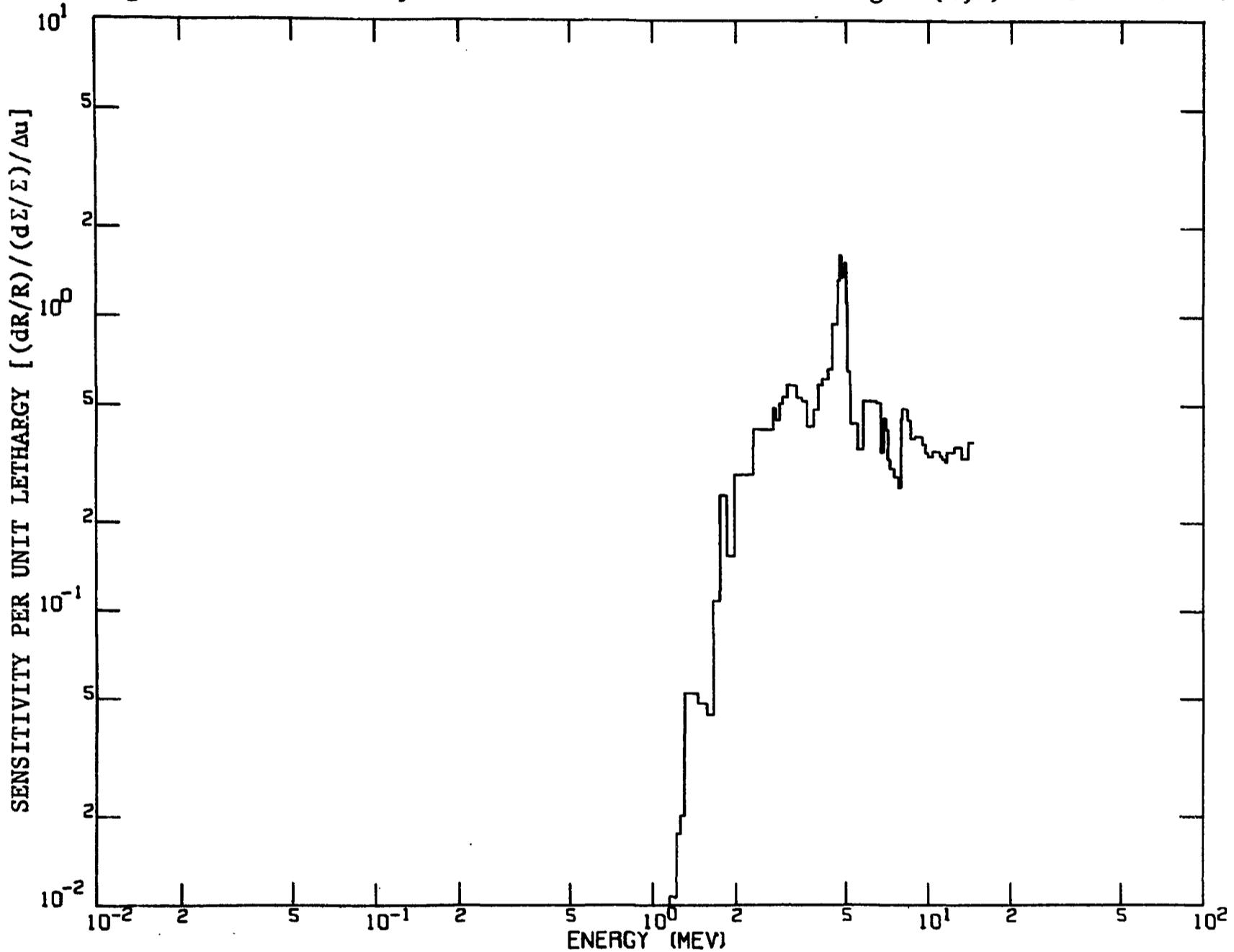
ORNL-DWG 72-12518

Fig. 11.   Sensitivity of Total Tissue Dose to Nitrogen (N,P) + (N,D) +
(N,T) Cross Sections.
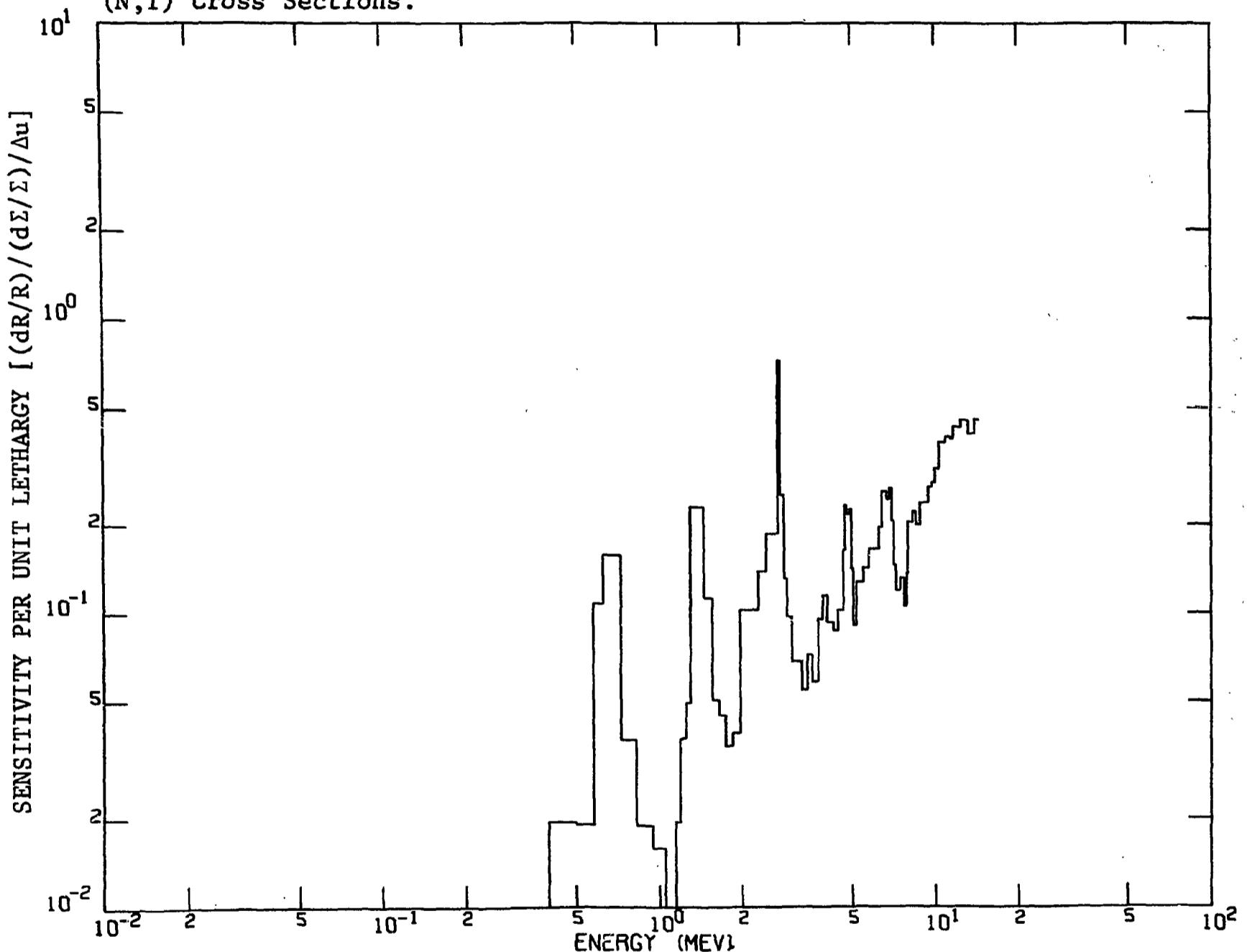
Fig. 12.   Sensitivity of Total Tissue Dose to Oxygen Neutron Total
Cross Section.
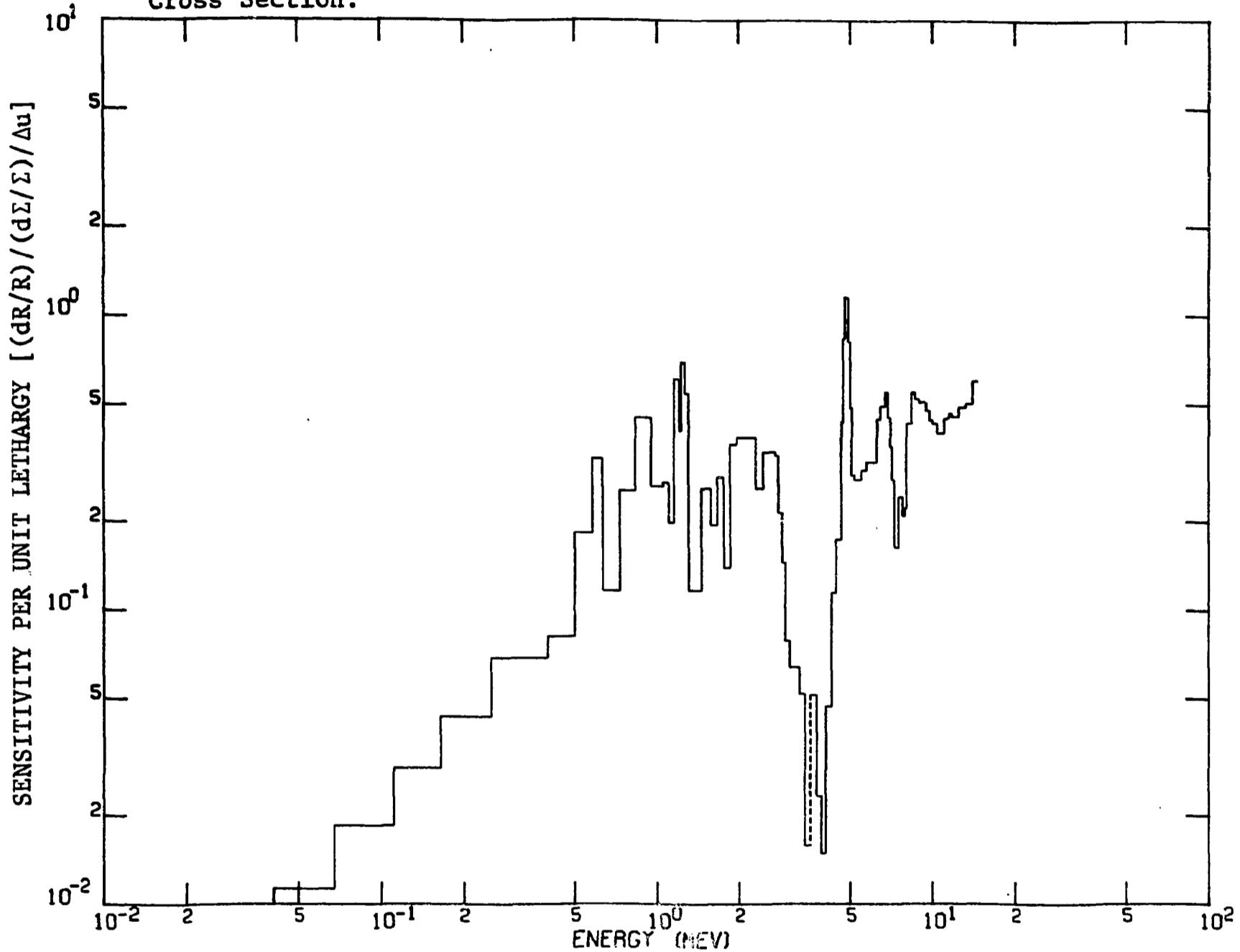
Figure (13) shows the sensitivity profile for oxygen elastic cross
sections and is included to show that the oxygen elastic cross sections
are responsible for all of the important areas of sensitivity in Fig. (12),
even in the 5 MeV nitrogen minimum where absorption effects might be
expected to dominate.

Fig. 13. Sensitivity of Total Tissue Dose to Oxygen Neutron Total
Cross Section.
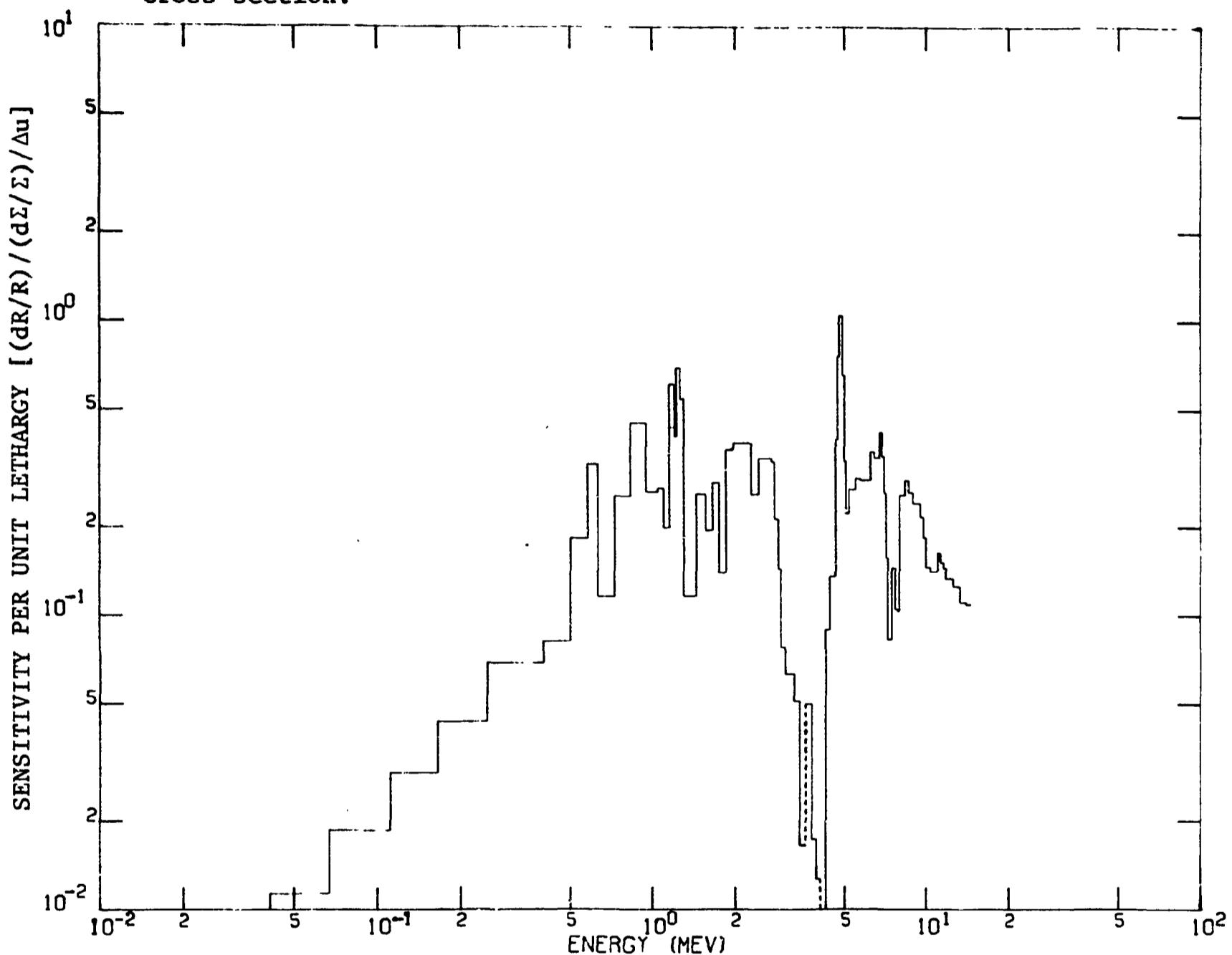
E. Prediction - Calculation Comparisons

The sensitivity approach described here may also be used as a basis
for prediction of changes in the tissue dose due to changes in the cross
sections utilized in the calculation. Since such predictions are based
on linear perturbation theory, it is desirable to have an idea of the
range of linearity for the problem under study before illustrating the
predictive aspect of the analysis with further example. Table II presents
a comparison between predicted and calculated changes in the tissue dose
resulting from density-type perturbations in the indicated cross sections
(a uniform percent change in the cross sections at all energies). The
predicted values in Table II were obtained from the sensitivities given
in Table I by multiplying the predicted percent change in the tissue dose
due to a 1% change in a specific cross section set by the percent change
selected for that cross-section set. The calculated values in Table II
were obtained by making the indicated changes in the cross sections and
rerunning the original ANISN calculation. The agreement between prediction
and calculation is reasonably good for small changes in the dose (up to
about 20%) but becomes poorer for larger changes (for example around 60%)
showing an increasing nonlinearity for increasing perturbations. Both
positive and negative perturbations were included to indicate that the
predicted results tend to be too high for a cross section increase and
too low for a cross section decrease for this problem. It is interesting
to note, however, that the predicted change falls very close to the average
absolute magnitude of the calculated changes in dose resulting from cross
section increases and decreases

The predictive aspect of this sensitivity study may be applied to
predicting the number of Legendre expansion moments needed to represent
the scattering kernel. By viewing the perturbation to be made as a reduction
in the number of moments representing the scattering transfer cross section,
predictions may be made of the effect of running this calculation with a
different number of moments. The first three cases in Table III show the
predicted and calculated effects of running this calculation, which was
originally run P_3, as a P_2, P_1, or P_0 calculation. The comparison between
predicted and calculated changes shows the increasing nonlinearity noted in

Table II. Predicted vs Calculated Variation of the Tissue Dose

Due to Cross-Section Perturbations

Cross-Section Perturbation in Σ Collision (%)	Elements	Predicted Change in Tissue Dose (%)	Calculated Change in Tissue Dose (%)
+1.0	N_2+O_2	-7.50	-7.13
-1.0	N_2+O_2	+7.50	+7.69
+10.0	O_2	-14.2	-13.1
-10.0	O_2	+14.2	+15.2
+5.0	N_2	-30.4	-25.8
-5.0	N_2	+30.4	+35.2
+10.0	N_2	-60.8	-44.8
-10.0	N_2	+60.8	+83.1

Table III. Predicted vs Calculated Variation of the Tissue Dose

With Number of Legendre Moments Used in the Angular Expansion

Number of Moments	Energy Group		Predicted Change in Tissue Dose From Initial P_3 (%)	Calculated Change in Tissue Dose From Initial P_3 (%)
	Neutron	Gamma		
P_2	all groups	all groups	+0.18	+0.13
P_1	all groups	all groups	-8.2	-6.1
P_0	all groups	all groups	-95	-55.9
P_3	1-8	1-14		
P_2	9-68	15-28	-0.015	+0.063
P_1	69-101	29-33		

Table II. However, the general conclusions that a P_2 result is very close to the P_3 answer and a P_1 calculation is fairly close, while a P_0 answer is in poor agreement with the P_3 result, are stated quite clearly by the predicted quantities in Table III. As an example of the usefulness of this type of information, the preliminary air sensitivity investigation referred to earlier was changed from a P_5 to a P_3 calculation with a resulting deviation of only +0.03% in the total tissue dose as the result of a study similar to that shown in Table III. In addition to considering P_ℓ changes for all energy groups at one time, it is feasible to determine P_ℓ requirements as a function of group. The fourth entry in Table III represents a P_ℓ truncation by group predicted to give approximately equal dose changes for each group, with a total change of about 0.05%. Although most discrete ordinates transport codes are not currently able to handle a variation in the number of Legendre moments by group, such calculations might be advantageous, especially in terms of input-output time requirements for two-dimensional codes. It should be noted that the P_0 calculations mentioned here used an S_{16} Gaussian Legendre quadrature and so are not equivalent to diffusion calculations.

IV. ESTIMATES OF UNCERTAINTIES

An estimation of the uncertainty in the calculated result (tissue dose for this problem) due to estimated uncertainties in the evaluated cross sections used in the calculation is potentially one of the most useful aspects of the approach to sensitivity studies described here. In applying the methods described in Section II to uncertainty analysis, the estimated uncertainties in the evaluated cross section are viewed as the cross section perturbations to be considered. The change in the calculated result predicted by linear perturbation theory is then an estimate of the uncertainty in the calculation resulting from the evaluated uncertainties in the cross sections utilized. Such estimates not only aid in establishing a level of confidence in the calculation, but also identify the reactions and energy ranges where cross section uncertainties are most important for the given problem. This information may subsequently be used to guide the remeasurement and reevaluation of specific cross section sets in order to improve confidence in the calculation.

Since the evaluator can provide estimates of the magnitude of the uncertainties in a given set of cross section, there is no sign associated with these uncertainties, and the linear perturbation approach is therefore especially applicable here since it requires only the magnitude, not sign, of the proposed cross section perturbations. By comparison, a direct recalculation with perturbed cross sections requires both the magnitude and sign of the perturbations, as well as a statement of the correlation between the cross section uncertainties. Using direct methods therefore makes the question of considering the total effect of all uncertainties quite complex and fairly arbitrary, as well as being very time consuming. However, direct recalculation is certainly advantageous in determining exact effects of cross sections uncertainties known to be very important, especially if these effects are of sufficient magnitude to be well beyond the range of accuracy for linear perturbation theory.

In addition to estimates of cross section uncertainties, it is also necessary to have information concerning the interrelation of the cross section sets used in the calculation. For example, if the nitrogen inelastic cross section at a given energy has an estimated uncertainty of 20%, one must know whether or not there is any correlation with an uncertainty in the nitrogen elastic cross section at that energy. A rigorous mathematical approach would involve using covariance matrices to describe the correlations by energy and nuclide between all the cross sections used in the calculation. These covariance matrices express the degree of correlation between cross sections, and would be based on experimental effects such as normalization, resolution, and the use of cross section standards. Although such covariance matrices are not available at this time, the Error Subcommittee of the Cross Section Evaluations Working Group (CSEWG) has developed formats to handle them[24] and hopefully some of these will be available in the future.

Presently, some information on cross section uncertainties is available in reports dealing with the current evaluations for nitrogen[25] and oxygen.[26] These reports contain rough error files which give estimated uncertainties for most of the evaluated cross sections at selected neutron

energies. The evaluators state that these estimates are approximate in
nature and do not reflect exact, detailed information. Nevertheless, they
represent the best information currently available concerning nitrogen and
oxygen cross section uncertainties, and so were utilized as the basis for
the calculations of estimated uncertainties presented here.

Table IV shows some estimates of uncertainties in nitrogen neutron
cross sections which were obtained from Ref. 18. The uncertainty in the
total cross section is quite low, as is the uncertainty in the elastic
cross section at lower energies. At higher energies the elastic cross
section is less well known. The various nonelastic reaction cross sections
all have large to very large uncertainties except in the thermal range.
The values given in Table IV represent uncertainties in measured or cal-
culated cross section sets. However the evaluators state that the nitrogen
elastic cross sections in the ENDF/B-III listing below 10 MeV were derived
from the total cross section and the sum of all nonelastic cross sections
according to Eq. (47). Below 10 MeV

$$\sigma_{elastic} = \sigma_{total} - \sigma_{nonelastic} \tag{47}$$

Above 10 MeV, the inelastic cross section was derived from the total,
elastic, and other nonelastic cross sections shown as $\sigma'_{nonelastic}$ in Eq. (48).

$$\sigma_{inelastic} = \sigma_{total} - \sigma_{elastic} - \sigma'_{nonelastic} \tag{48}$$

where

$$\sigma_{nonelastic} = \sigma_{inelastic} + \sigma'_{nonelastic} \tag{49}$$

In order to obtain an estimate of the uncertainty in the calculated
dose resulting from the nitrogen cross section uncertainties given in
Table IV, it was first necessary to assume that the uncertainties listed
at a given energy extended to energy boundaries halfway between the listed
midpoints. For example, the uncertainties listed at 2 MeV were assumed
to extend from 1.5 MeV to 3.5 MeV. This assumption was made for all
midpoint values given except that the .1 MeV values were assumed to
extend down in energy to the thermal group. The percent uncertainty in

Table IV. Estimated Percent Uncertainty in the Evaluated Nitrogen Neutron Cross Sections
(From Reference 25)

Cross Section	Midpoint of Energy Range (MeV)							
	Thermal	.1	1	2	5	8	11	14
Total	3	3	1	1	1	1	1	1
Elastic	3	3	1	1	10	10	15	10
Inelastic					30	20	20	20
(n,γ)	10	400	400	400	200	200	200	200
$(n,d)+(n,p)+(n,t)$	5	30	30	30	30	40	40	30
(n,α)				40	30	30	30	30
$(n,2\alpha)$								50
$(n,2n')$								20

a cross section at a given energy was then multiplied by the percent change in dose per percent change in cross section at that energy perdicted by linear perturbation theory. In order to see the full effect of a particular uncertainty, it was also necessary to consider resulting uncertainties in the derived cross section as indicated by Eqs. (47) and (48). For example, to determine the effect of the uncertainty in the (n,α) cross section in an energy group near 5 MeV, one must consider that the (n,α) uncertainty is inversely reflected in the elastic cross section.

The uncertainty in the (n,α) cross section at 5 MeV must then be compensated for by an associated uncertainty in the elastic cross section in order to satisfy Eq. (47) and maintain a consistent total cross section. The predicted effect on the tissue dose must then be the combination of the predicted effects due to the (n,α) and associated elastic cross section uncertainties. Below 10 MeV, uncertainties in all nonelastic cross sections were compensated for by associated uncertainties in the elastic cross section. Above 10 MeV where the inelastic cross section was derived according to Eq. (48), both the elastic and the other nonelastic cross section uncertainties were compensated for by associated uncertainties in the inelastic cross section, According to Eqs. (47) and (48) an uncertainty in the total cross section appears as an uncertainty in the derived cross section. The predicted effect on the dose of the uncertainty in the total cross section was therefore taken to be the predicted effect of an equivalent uncertainty in the elastic cross section for energies under 10 MeV and in the inelastic cross section for energies above 10 MeV. The above procedures assume that the measured or calculated cross sections have a covariance of ±1 with the derived cross section at a given energy (+1 for total, -1 for all others).

Table V presents the estimated uncertainty in the calculated tissue dose due to the estimated uncertainties in the nitrogen neutron cross sections given in Table IV. It should be noted that the dose uncertainties given here do not include the effects of cross section uncertainties in secondary energy and angular distributions. The values given for all measured or calculated cross sections include the effects of compensation

Table V. Estimated Percent Uncertainty in Total Tissue Dose
Due to Estimated Uncertainty in Nitrogen Neutron Cross Sections

Cross Section	Midpoint of Energy Range (MeV)								Sum Over All Energy Ranges
	Thermal	.1	1	2	5	8	11	14	
Total	0.0006	0.700	0.599	1.09	0.501	0.424	0.896	0.542	4.75 Corr
Elastic	0.603*	2.47*	1.91*	8.98*	10.59*	4.73*	6.71	2.62	9.33 Corr > 10 MeV
Inelastic				0.017	1.15	2.04	6.92*	2.84*	3.21 Corr < 10 MeV
(n,γ)	0.53	0.63	0.02	0.024	0.006	0.004	0.00	0.00	1.21 Corr
$(n,d)+(n,p)+(n,t)$	0.287	2.28	1.79	2.33	1.92	2.35	1.13	0.703	12.79 Corr
(n,α)			0.284	8.60	10.34	3.54	0.86	0.54	24.16 Corr
$(n,2\alpha)$							0.045	0.345	0.39 Corr
$(n,2n)$							0.002	0.017	0.02 Corr

Estimated overall calculational uncertainty due to Table IV uncertainties in neutron cross sections   *29.48

*Uncorrelated summation of the uncertainties due to all measured cross sections for the designated energy range.

with the derived cross sections as discussed previously. The value given for the derived cross sections are identified by an astrisk and represent the square root of the sum of the squares of the dose uncertainties due to uncertainties in all measured or calculated cross section sets in the indicated energy range. This determination of the uncertainty in the derived cross section assumes that there is no correlation between any of the measured cross section sets. The values given for the individual reaction cross sections as a sum over all energies is a simple numerical sum of the values for the various energy ranges, which assumes a complete correlation over all energies for measured quantities. The summed values given for the elastic and inelastic cross sections were obtained by summing over the energies where measured values were used for these cross sections. The value given as the estimated overall calculational uncertainty represents the uncorrelated sum of the tissue dose uncertainties for all of the nitrogen reaction cross sections given. The dominance of the effect of the (n,α) cross section is due to a combination of large uncertainty (see Table IV) and high sensitivity (see Fig. 10), especially in the energy region between 6.5 and 2 MeV. This high sensitivity is due to the relatively large (n,α) cross section in the energy region covering the major nitrogen and oxygen minima in the total cross section, most notably around the 4.9 MeV nitrogen minimum. The effects of uncertainties in the (n,p), (n,d), and (n,t) cross sections, and in the elastic cross section above 10 MeV are significant but of secondary importance.

The estimated overall calculational uncertainty is not significantly affected by the uncertainties in the oxygen neutron cross sections and in the nitrogen and oxygen gamma cross sections, as would be expected from the sensitivities given in Table I. However, estimates of the effects of these uncertainties will be presented here for the sake of completeness. Table VI presents estimated uncertainties in oxygen neutron cross sections as given by the evaluators in Ref. 26 . The general features of Table VI are similar to those of Table IV for the nitrogen neutron cross sections in that the total cross section is well known, the elastic cross section is well known except at higher energies, and the nonelastic cross sections are less known. The evaluated oxygen elastic cross sections below 11 MeV

Table VI. Estimated Percent Uncertainty in the Evaluated Oxygen Neutron Cross Sections

(From Reference 26)

Cross Section	Midpoint of Energy Range (MeV)							
	Thermal	.1	1	3	5	8	11	14
Total	4	4	1	1	1	1	1	1
Elastic	4	4	1	1	3	6	15	10
Inelastic						30	30	30
(n,γ)	14%	lower limit only ⟶						
(n,α)				20	20	20	20	20
(n,p)							20	20
(n,d)							50	30

were derived from the total cross section and the sum of all nonelastic cross sections according to Eq. (47), as were the nitrogen elastic cross sections below 10 MeV. The oxygen inelastic cross section above 11 MeV was derived from the total, elastic, and other nonelastic cross sections in the manner indicated by Eq. (48). The uncertainty values were assumed to extend to energy boundaries halfway between the stated energy midpoints, except that the thermal value was restricted to the thermal group. In computing the estimated uncertainties in the tissue dose below 11 MeV, the uncertainties in all nonelastic cross sections were compensated for by associated uncertainties in the elastic cross sections. Above 11 MeV, the elastic and the other nonelastic cross section uncertainties were compensated for by associated uncertainties in the inelastic cross section. The uncertainty in the total cross section was taken as an uncertainty in the elastic cross section below 11 MeV and as an uncertainty in the inelastic cross section above 11 MeV. Table VII presents the estimated uncertainty in the calculated tissue dose due to the estimated uncertainties in the oxygen neutron cross sections given in Table VI. As in Table IV, the uncertainty values for all measured or calculated cross sections include the effects of compensation with the derived cross section, and the derived cross section, indicated by an asterisk, represent the uncorrelated sum of the dose uncertainties due to all measured or calculated cross sections in the given energy range. The uncertainties are assumed to be correlated over all energies for a given measured or calculated cross section and to be uncorrelated between measured cross sections. The estimated overall calculational uncertainty is small, with the primary contribution coming from the total cross section at lower energies, and secondary contributions from the (n,α) and inelastic cross sections in the energy regions with midpoints at 8 MeV and at 11 MeV.

The gamma transport cross sections are considerably better known than the neutron transport cross sections. According to J. H. Hubbell,[27] gamma transport cross sections for low-Z materials, such as nitrogen and oxygen, are in general known to within about 1% in the energy range from 0.03 MeV to 100 MeV, especially in energy regions where gamma transport is dominated by the Compton reaction. Since the energy range of gammas

Table VII. Estimated Percent Uncertainty in Total Tissue Dose
Due to Estimated Uncertainty in Oxygen Neutron Cross Sections

Cross Section	Midpoint of Energy Range (MeV)								Sum Over All Energy Ranges
	Thermal	.1	1	3	5	8	11	14	
Total	0.0004	0.995	0.871	0.170	0.317	0.281	0.181	0.190	3.01 Corr
Elastic	0.0004*	0.995*	0.871*	0.173*	0.421*	0.872*	0.941*	0.467	0.47 Corr > 12.5 MeV
Inelastic						0.619	0.636	0.553*	1.26 Corr < 12.5 MeV
(n,γ)	0.0000								0.00 Corr
(n,α)				0.031	0.277	0.546	0.663	0.212	1.73 Corr
(n,p)							0.086	0.074	0.16 Corr
(n,d)							0.027	0.042	0.07 Corr

Estimated overall calculational uncertainty due to Table VI uncertainties
in oxygen neutron cross sections   *3.73

51

*Uncorrelated summation of the sensitivity to all measured cross sections for the designated energy range.

transported in this calculation went from 10 MeV to 0.0101 MeV, it was felt that assuming an uncertainty of 2% in all gamma transport cross sections was fairly conservative. A slightly conservative estimate in gamma transport cross section uncertainty seems acceptable since they are well known and can only affect the gamma tissue dose which is about 27% of the total tissue dose. All gamma cross section uncertainties were assumed to be completely correlated, between elements as well as for an individual element. The results are stated in Table VIII, showing a small resulting uncertainty in the calculated total tissue dose as expected. Table IX shows the total estimated uncertainty in the calculated tissue dose due to estimated uncertainties in the cross sections used in the calculation. It should be emphasized that these results are not intended as exact limits on the accuracy of this calculation. The accuracy of the estimated uncertainty in the calculated result is limited by the detail and accuracy to which cross section uncertainties and covariances are known, and by the linear perturbation approximation. However, the approach used here does indicate specific cross section sets and energy regions where current cross section uncertainties are important. In the problem considered here, the nitrogen (n,α) cross section emerges as being of special importance, and the desirability of obtaining more accurate values for this cross section, especially in the 2 MeV to 6 MeV range, is evident. The estimate of the total uncertainty in the calculated tissue dose due to estimated uncertainties in all cross sections as detailed previously is given in Table IX as approximately 30%, while the calculated dose uncertainty due to the nitrogen (n,α) cross section uncertainties is given in Table V as about 24%.

V. CONCLUSIONS

The cross-section sensitivity analysis procedure illustrated in this report is capable of indicating which cross sections, and therefore which physical processes, are important for a given calculation. In the case of the air transport problem considered here, the sensitivity profiles show that nitrogen inelastic cross sections dominate above 10 MeV, nitrogen elastic cross sections dominate below 2.5 MeV, and nitrogen absorption

Table VIII. Estimated Percent Uncertainty in the Calculated Total
(Neutron + Gamma) Tissue Dose Due to an Assumed 2% Uncertainty
in Gamma Transport Cross Sections

Element for Gamma Transport Cross Section Uncertainty	Estimated Percent Uncertainty in the Calculated Tissue Dose
N_2	1.66
O_2	0.52
$N_2 + O_2$	2.18

Table IX. Estimated Percent Uncertainty in the Calculated Total
Tissue Dose Due to Estimated Uncertainties
in the Cross Sections Used in the Calculation

Estimated Uncertainties in Cross Sections for	Estimated Percent Uncertainty in the Calculated Total Dose
N_2 neutrons*	29.48
O_2 neutrons**	3.73
(N_2+O_2) gammas	2.18
(N_2+O_2) neutrons + gammas	29.79

*As given in Table IV.

**As given in Table VI.

cross sections are important above 2.5 MeV, especially the (n,α) cross section in the vicinity of 5 MeV.

The use of linear perturbation theory permits the treatment of variations in measured cross section uncertainties and correlations with nonmeasured cross sections as a function of energy group. In addition, the linear-perturbation predictions of changes in the total tissue dose as the result of cross-section changes agree well enough with direct substitution calculations to permit the estimation of the effects of cross section uncertainties on the uncertainty in the calculated tissue dose, and to identify cross sections for possible remeasurement. The estimated overall uncertainty in the tissue dose for this air transport problem due to cross section uncertainties is about 30%, and the need for remeasuring the nitrogen (n,α) cross section is indicated, especially in the neighborhood of 5 MeV.

APPENDIX A

In this appendix the unclassified thermonuclear neutron source,[18] the Snyder-Neufeld[21] neutron tissue dose response function, and the Henderson[22] gamma tissue dose response function are presented along with the 129-neutron, 42-gamma energy group structure utilized in the calculation.

Table A1. Neutron Energy Group Structure, Unclassified Thermonuclear Source, and Snyder-Neufeld Tissue Dose Response Functions

Neutron Energy Group	Upper Energy Bound (MeV)	Unclassified Thermonuclear Source (Neutrons)	Snyder-Neufeld Tissue Dose Response Functions (Rads/n/cm²)	Neutron Energy Group	Upper Energy Bound (MeV)	Unclassified Thermonuclear Source (Neutrons)	Snyder-Neufeld Tissue Dose Response Functions (Rads/n/cm²)
1	14.5	2.52(-2)	6.4(-9)	26	6.25	6.47753(-3)	6.2(-9)
2	14.0	1.89(-2)	6.5(-9)	27	5.75	2.97852(-3)	6.1(-9)
3	13.25	1.89(-2)	6.6(-9)	28	5.52	4.144(-3)	6.0(-9)
4	12.5	1.2837(-2)	6.7(-9)	29	5.2	1.82186(-3)	5.8(-9)
5	11.75	2.909(-3)	6.8(-9)	30	5.07	9.81(-4)	5.8(-9)
6	11.5	2.909(-3)	6.8(-9)	31	5.0	1.12115(-3)	5.8(-9)
7	11.25	2.909(-3)	6.9(-9)	32	4.92	2.27(-3)	5.5(-9)
8	11.0	6.98163(-3)	6.9(-9)	33	4.8	1.50934(-3)	5.4(-9)
9	10.4	4.65443(-3)	7.0(-9)	34	4.72	1.32067(-3)	5.4(-9)
10	10.0	1.95(-3)	7.0(-9)	35	4.65	3.775(-3)	5.3(-9)
11	9.75	1.95(-3)	7.0(-9)	36	4.45	2.835(-3)	5.2(-9)
12	9.5	4.674(-3)	7.1(-9)	37	4.3	3.78(-3)	5.2(-9)
13	8.9	2.337(-3)	7.1(-9)	38	4.1	3.506(-3)	5.1(-9)
14	8.6	1.949(-3)	7.2(-9)	39	3.95	3.68(-3)	5.0(-9)
15	8.35	2.77288(-3)	7.2(-9)	40	3.8	4.91(-3)	4.9(-9)
16	8.0	7.97147(-4)	7.2(-9)	41	3.6	3.68(-3)	4.9(-9)
17	7.9	1.2(-3)	7.1(-9)	42	3.45	3.68(-3)	4.8(-9)
18	7.75	2.01(-3)	7.0(-9)	43	3.3	6.13(-3)	4.7(-9)
19	7.5	2.01(-3)	6.9(-9)	44	3.05	3.50535(-3)	4.6(-9)
20	7.25	1.206(-3)	6.8(-9)	45	2.94	2.31117(-3)	4.6(-9)
21	7.1	8.04(-4)	6.8(-9)	46	2.87	3.10952(-3)	4.5(-9)
22	7.0	1.206(-3)	6.7(-9)	47	2.78	2.073(-3)	4.4(-9)
23	6.85	1.259(-3)	6.7(-9)	48	2.72	9.87436(-3)	4.3(-9)
24	6.7	2.457(-3)	6.5(-9)	49	2.45	7.05272(-3)	4.3(-9)
25	6.43	1.638(-3)	6.5(-9	50	2.3	1.75141(-2)	4.2(-9)

Table Al (cont'd)

Neutron Energy Group	Upper Energy Bound (MeV)	Unclassified Thermonuclear Source (Neutrons)	Snyder-Neufeld Tissue Dose Response Functions (Rads/n/cm^2)	Neutron Energy Group	Upper Energy Bound (MeV)	Unclassified Thermonuclear Source (Neutrons)	Snyder-Neufeld Tissue Dose Response Functions (Rads/n/cm^2)
51	1.97	6.46(-3)	4.2(-9)	76	2.478(-2)	6.73(-2)	6.7(-10)
52	1.85	7.97(-3)	4.2(-9)	77	1.503(-2)	3.61(-2)	5.7(-10)
53	1.75	7.74693(-3)	4.1(-9)	78	9.11(-3)	2.19(-2)	5.4(-10)
54	1.66	7.7531(-3)	4.1(-9)	79	5.53(-3)	1.33(-2)	5.3(-10)
55	1.57	1.03371(-2)	4.0(-9)	80	3.35(-3)	8.1(-3)	5.7(-10)
56	1.45	1.29156(-2)	4.0(-9)	81	2.03(-3)	4.9(-3)	6.0(-10)
57	1.3	3.44366(-3)	3.9(-9)	82	1.23(-3)	3.0(-3)	6.0(-10)
58	1.26	3.44366(-3)	3.9(-9)	83	9.61(-4)	1.0(-3)	6.0(-10)
59	1.22	1.72223(-3)	3.9(-9)	84	7.49(-4)	8.0(-4)	6.1(-10)
60	1.2	4.30558(-3)	3.9(-9)	85	5.83(-4)	1.205(-2)	6.3(-10)
61	1.15	4.96224(-3)	3.9(-9)	86	3.53(-4)	3.88(-3)	6.6(-10)
62	1.1	3.16252(-3)	3.8(-9)	87	2.75(-4)	5.38(-3)	6.8(-10)
63	1.05	9.74254(-3)	3.8(-9)	88	1.67(-4)	3.29(-3)	6.9(-10)
64	9.5(-1)	1.0138(-2)	3.7(-9)	89	1.01(-4)	6.14(-4)	6.9(-10)
65	8.3(-1)	8.5871(-3)	3.7(-9)	90	7.89(-5)	8.64(-4)	6.7(-10)
66	7.3(-1)	2.15(-2)	3.6(-9)	91	4.78(-5)	5.22(-4)	6.3(-10)
67	6.3(-1)	1.51668(-2)	3.3(-9)	92	2.9(-5)	0.0	6.1(-10)
68	5.8(-1)	8.83065(-3)	2.9(-9)	93	1.76(-5)	0.0	5.8(-10)
69	5.0(-1)	2.72529(-2)	2.6(-9)	94	1.067(-5)	0.0	5.6(-10)
70	4.0(-1)	1.39(-2)	2.3(-9)	95	6.47(-6)	0.0	5.3(-10)
71	2.5(-1)	3.48(-2)	2.0(-9)	96	3.93(-6)	0.0	5.1(-10)
72	1.65(-1)	1.97(-2)	1.6(-9)	97	2.38(-6)	0.0	4.9(-10)
73	1.11(-1)	1.25(-2)	1.3(-9)	98	1.44(-6)	0.0	4.7(-10)
74	6.73(-2)	2.042(-1)	1.0(-9)	99	8.76(-7)	0.0	4.5(-10)
75	4.086(-2)	1.26(-1)	8.1(-10)	100	5.31(-7)	0.0	4.3(-10)
				101	4.14(-7)	0.0	4.0(-10)
					1.0(-11)		

Table A2. Gamma Ray Energy Group Structure
and Henderson Tissue Dose Response Function

| Gamma Ray Energy Group	Upper Energy Bound (MeV)	Henderson Tissue Dose Response Function ($Rads/\gamma/cm^2$)
1	10.0	2.5(-9)
2	9.0	2.35(-9)
3	8.0	2.2(-9)
4	7.5	2.15(-9)
5	7.04	2.1(-9)
6	7.02	2.07(-9)
7	6.73	2.05(-9)
8	6.71	2.0(-9)
9	5.843	1.85(-9)
10	5.823	1.8(-9)
11	5.115	1.7(-9)
12	5.095	1.65(-9)
13	4.454	1.55(-9)
14	4.434	1.47(-9)
15	3.86	1.4(-9)
16	3.84	1.38(-9)
17	3.69	1.38(-9)
18	3.67	1.33(-9)
19	3.382	1.27(-9)
20	3.362	1.18(-9)
21	2.802	1.1(-9)
22	2.782	1.04(-9)
23	2.323	9.5(-10)
24	2.303	9.2(-10)
25	2.134	8.6(-10)
26	2.114	8.0(-10)
27	1.642	7.2(-10)
28	1.622	5.3(-10)
29	7.38(-1)	3.7(-10)
30	7.18(-1)	3.2(-10)
31	5.0(-1)	1.8(-10)
32	3.0(-1)	5.2(-11)
33	1.0(-1)	8.0(-11)
	1.01(-2)	

APPENDIX B

Additional sensitivity profiles are given in this appendix which show the sensitivity of the total tissue dose to nitrogen and oxygen neutron transport cross sections for specific reactions and to nitrogen and oxygen gamma transport cross sections. A list of the figures included in this appendix is given in Table B.1. Sensitivity profiles are not given for the tissue dose sensitivity to nitrogen (N,2N') and oxygen (N,γ) cross sections since the sensitivity to these cross sections was found to be very small.

Table B.1. List of Figures
(Profiles of Total Tissue Dose Sensitivity
to the Cross Section Types Indicated)

Figure No.	Element	Cross-Section Type
B.1	Nitrogen	(N,P)
B.2	"	(N,D)
B.3	"	(N,T)
B.4	"	(N,)
B.5	"	(N,2γ)
B.6	"	γ Transport
B.7	Oxygen	(N,N')
B.8	"	Absorption
B.9	"	(N,γ)
B.10	"	(N,P)
B.11	"	(N,D)
B.12	"	γ Transport

Fig. B. 1.   Sensitivity of Total Tissue Dose to Nitrogen (N,P) Cross Section
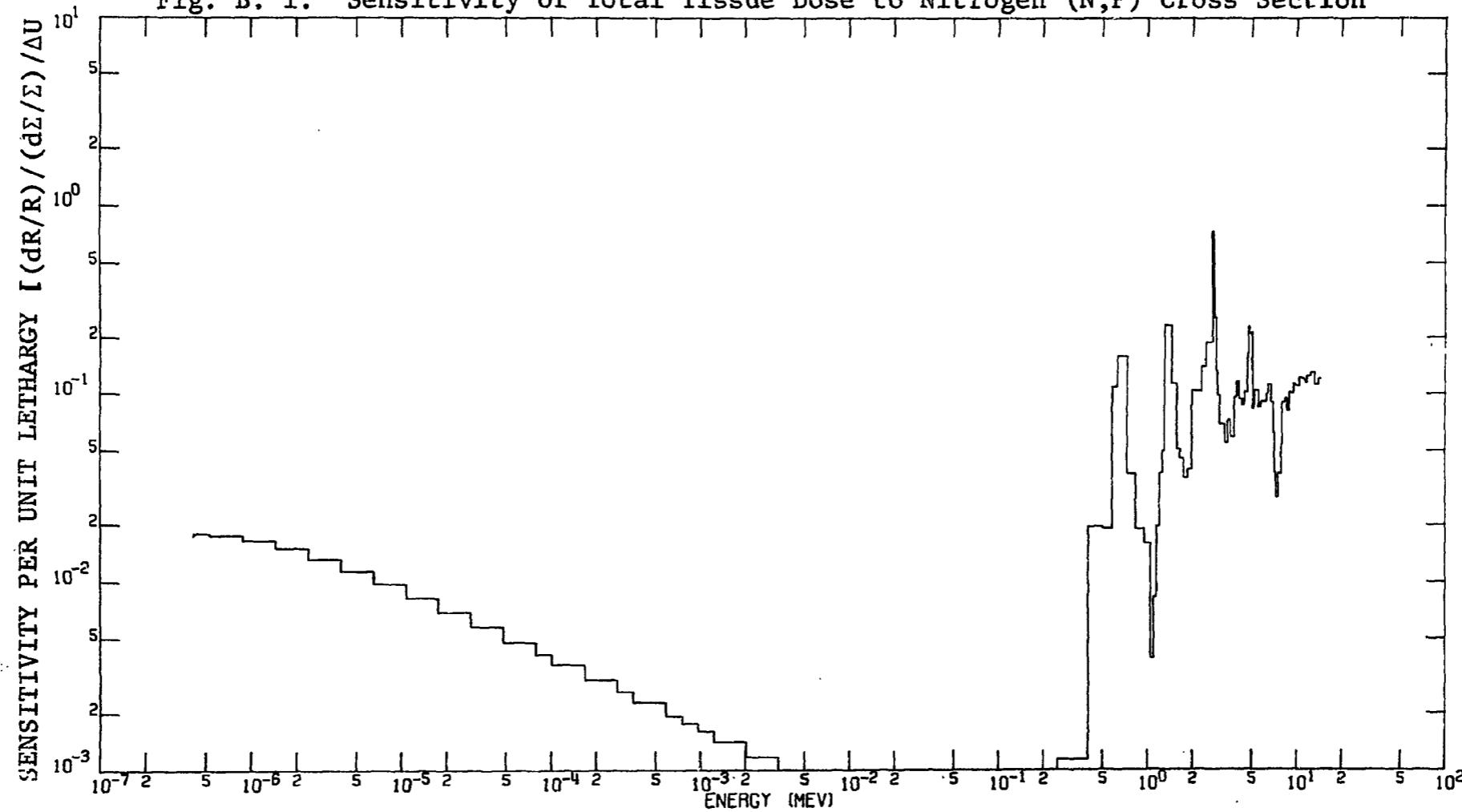
Fig. B.2. Sensitivity of Total Tissue Dose to Nitrogen (N,D) Cross Section
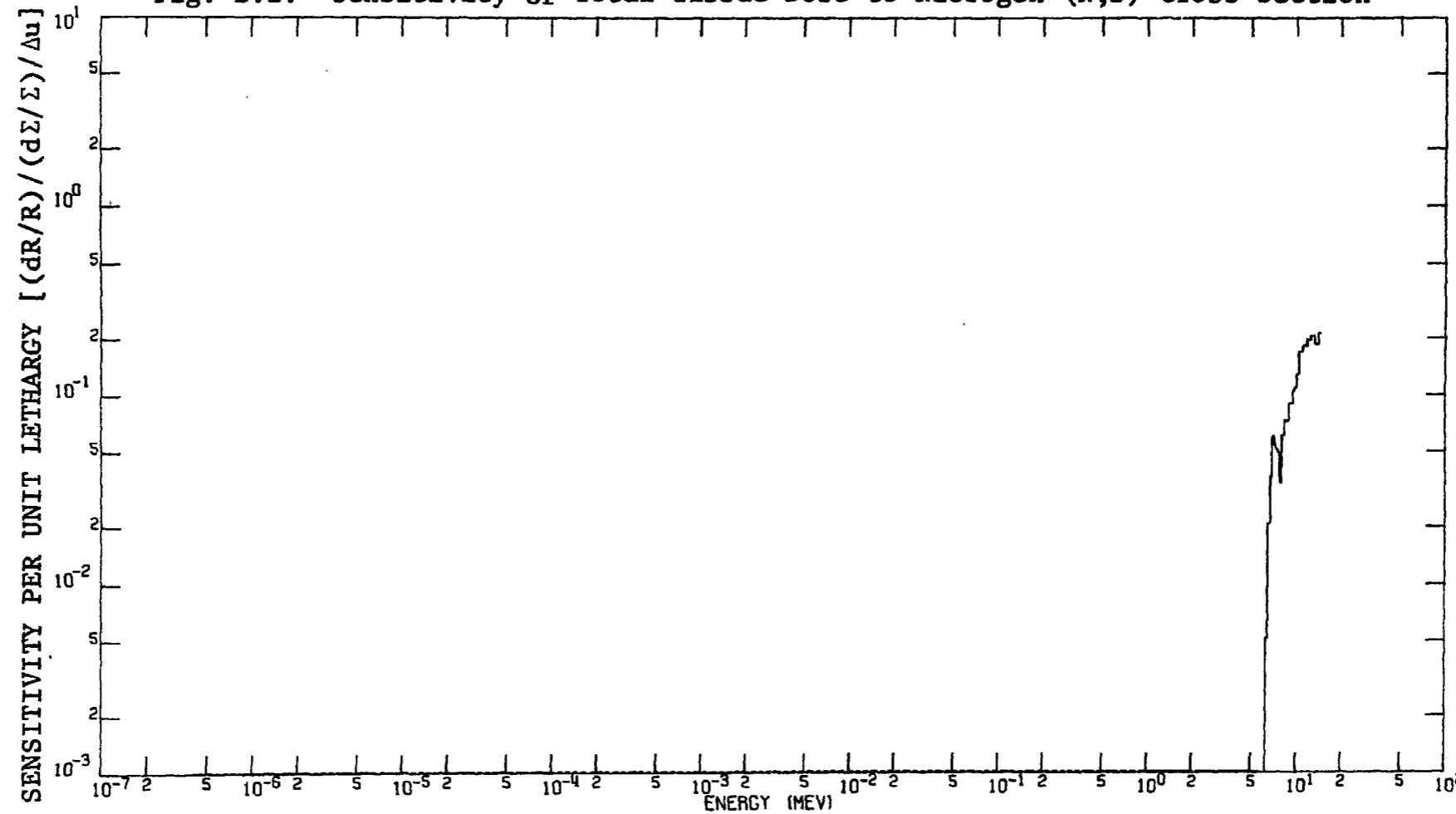
Fig. B.3. Sensitivity of Total Tissue Dose to Nitrogen (N,T) Cross Section
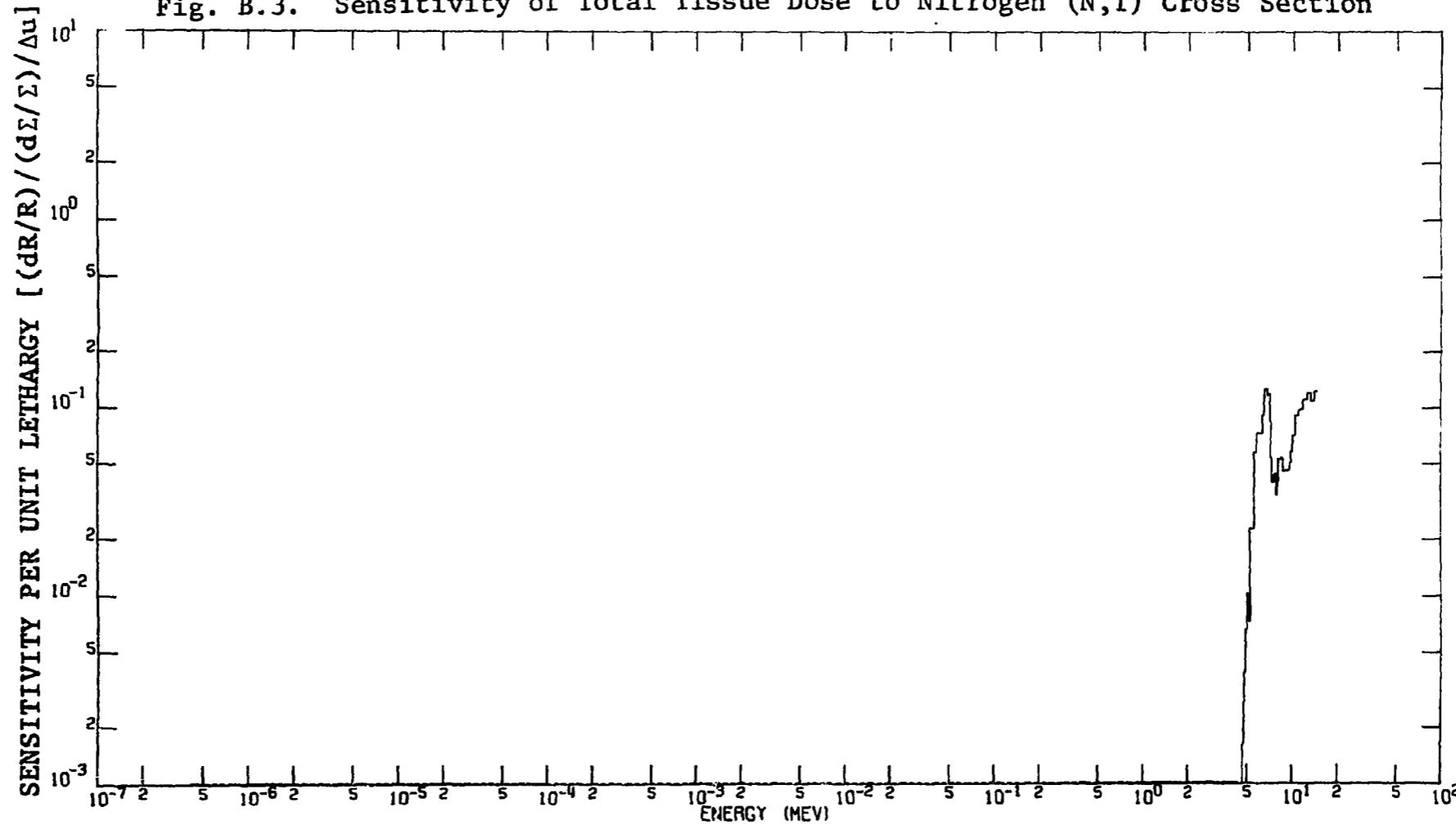
Fig. B.4. Sensitivity of Total Tissue Dose to Nitrogen (N,γ) Cross Section

ORNL-DWG 72-10966

SENSITIVITY PER UNIT LETHARGY [(dR/R)/(dΣ/Σ)/Δu]

ENERGY (MEV)

64
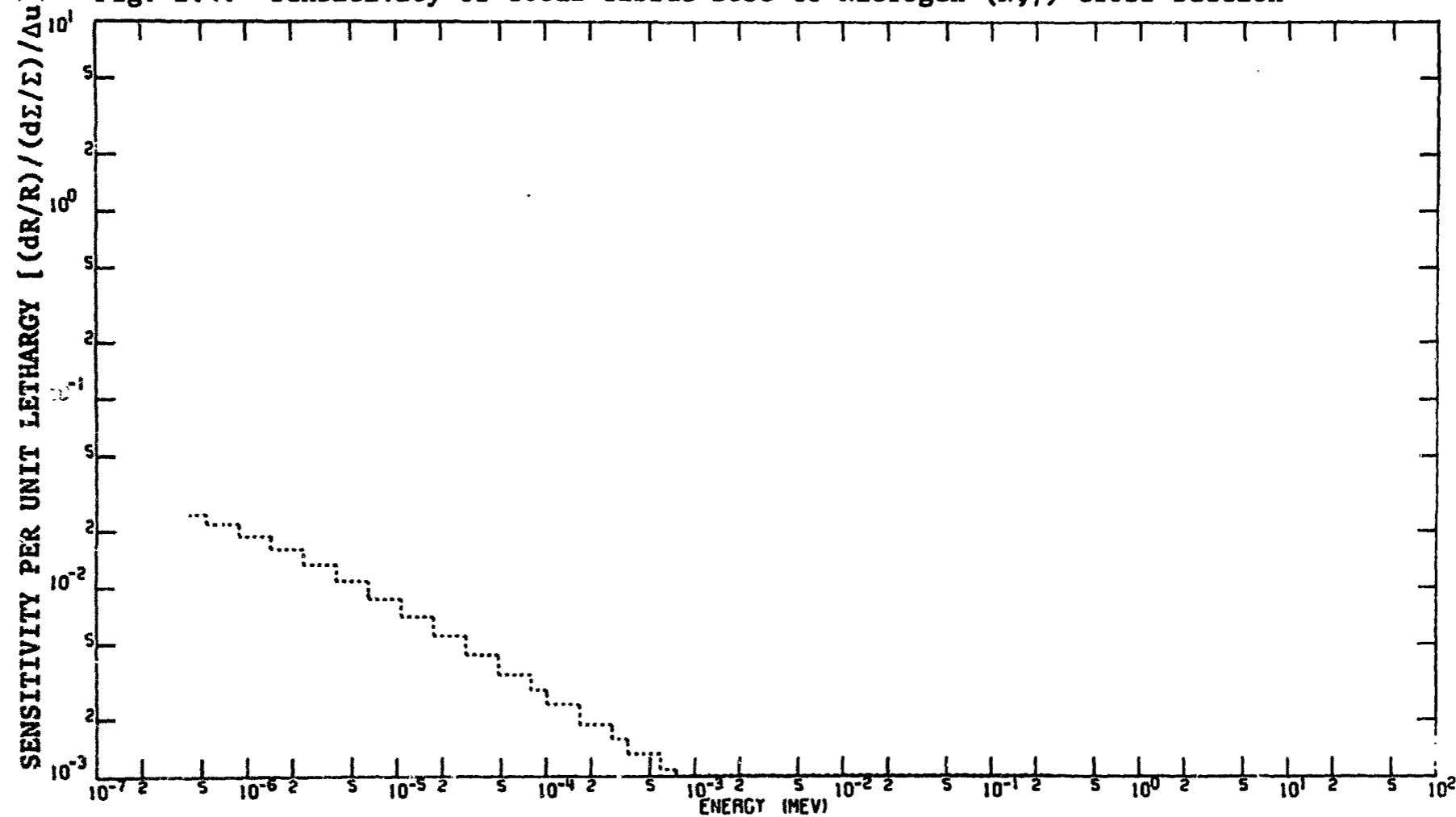
Fig. B.5. Sensitivity of Total Tissue Dose to Nitrogen (N,2α) Cross Section

SENSITIVITY PER UNIT LETHARGY [(dR/R)/(dΣ/Σ)/Δu]

ENERGY (MEV)
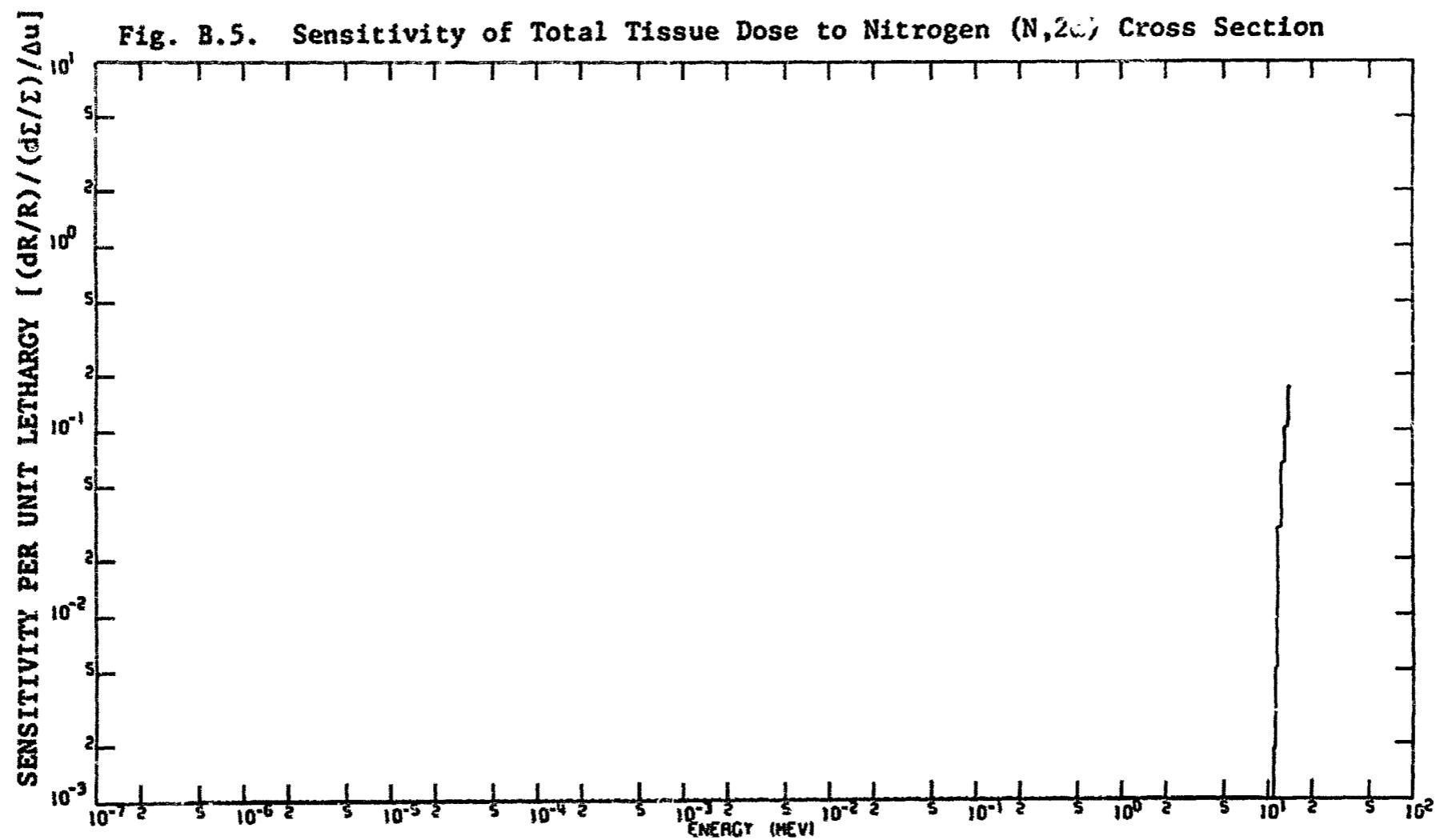
Fig. B.6. Sensitivity of Total Tissue Dose to Nitrogen Gamma Total Cross Section
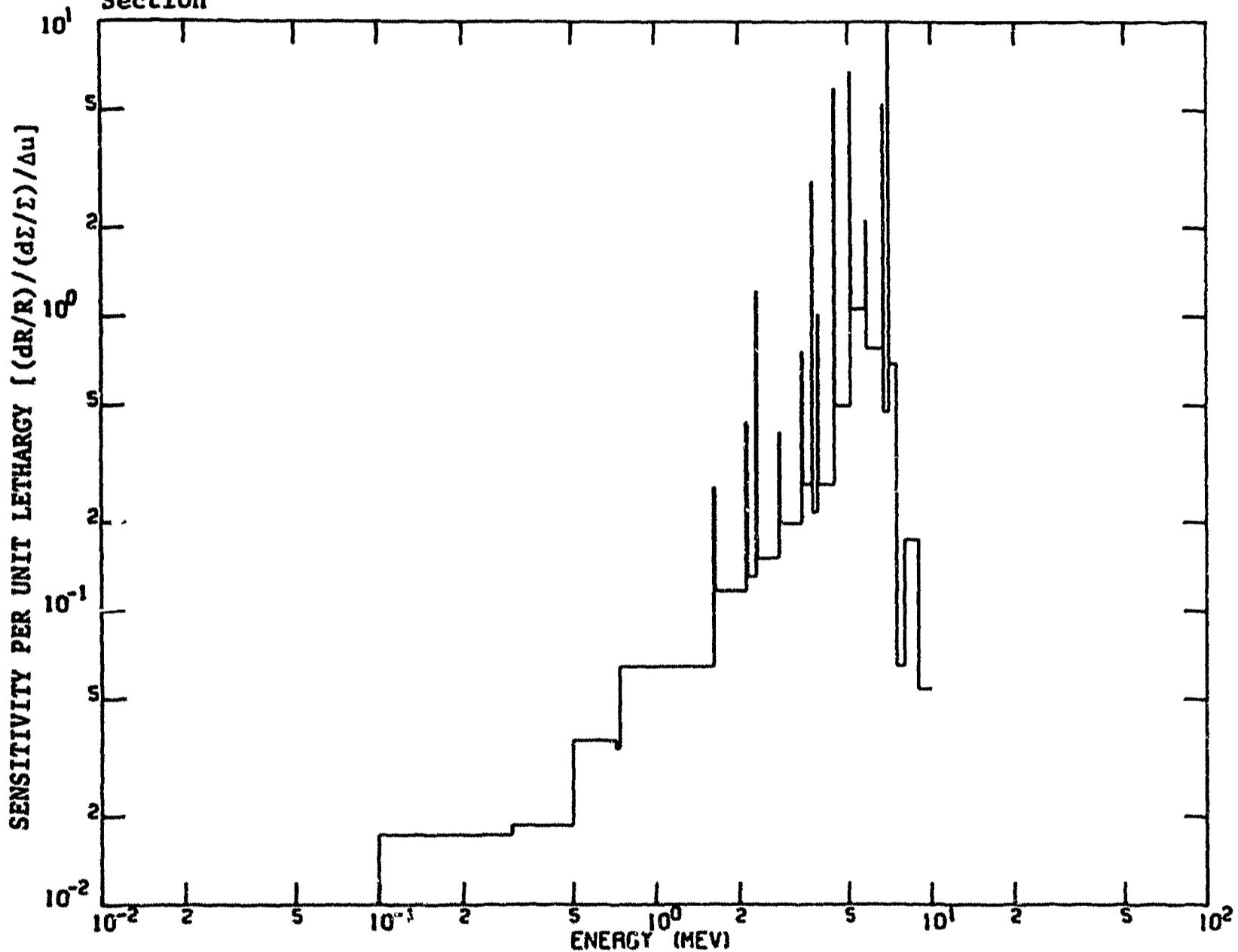
ORNL-DWG 73-4571

Fig. B.7. Sensitivity of Total Tissue Dose to Oxygen Neutron Inelastic Cross Section
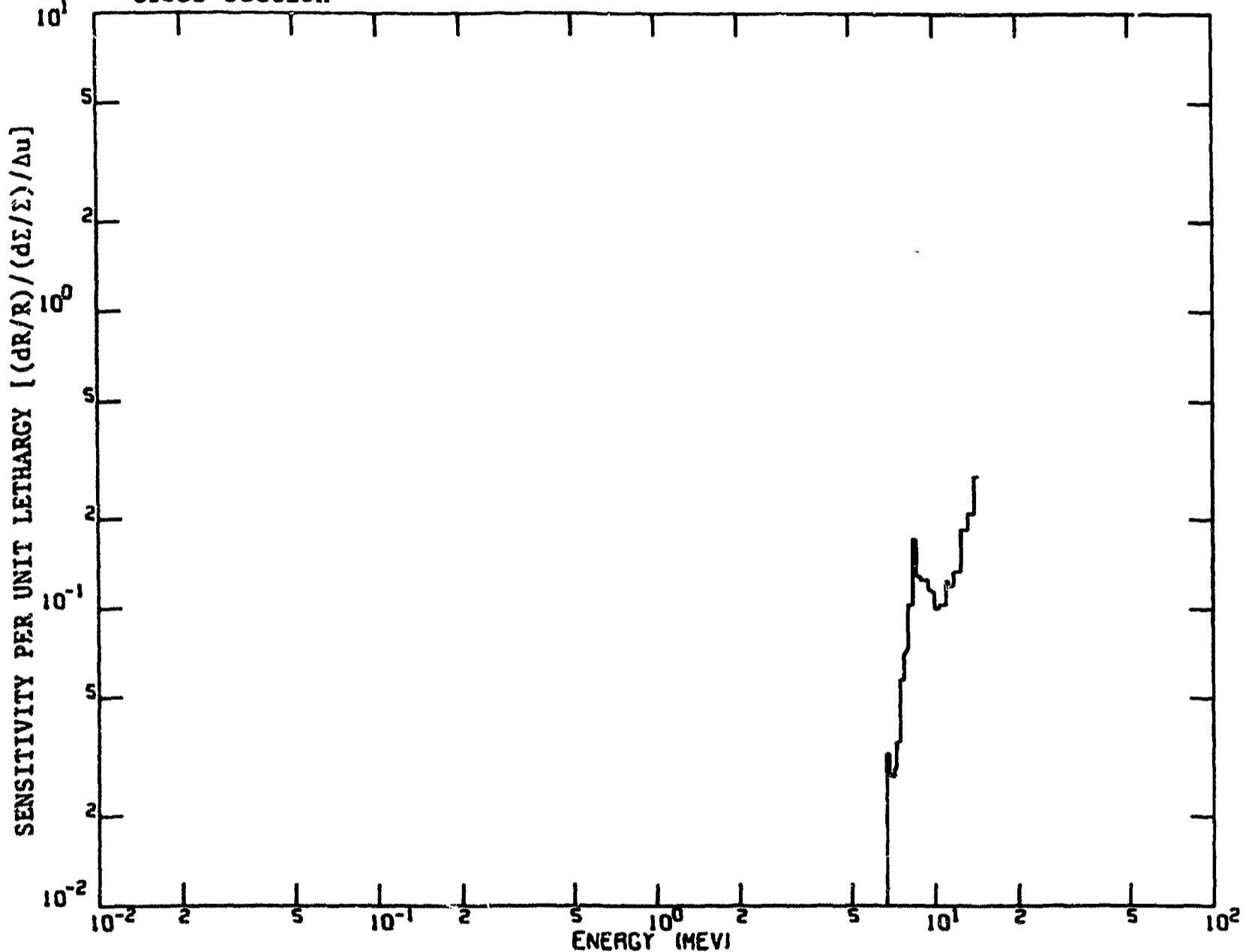
Fig. B.8.   Sensitivity of Total Tissue Dose to Oxygen Neutron Absorption
Cross Section

ORNL-DWG 73-4577

Fig. B.9. Sensitivity of Total Tissue Dose to Oxygen (N,α) Cross Section

Fig. B.10. Sensitivity of Total Tissue Dose to Oxygen (N,P) Cross Section

ORNL-DWG 72-10975

Fig. B.11. Sensitivity of Total Tissue Dose to Oxygen (N,O) Cross Section

ORNL-DWG 72-10973

71
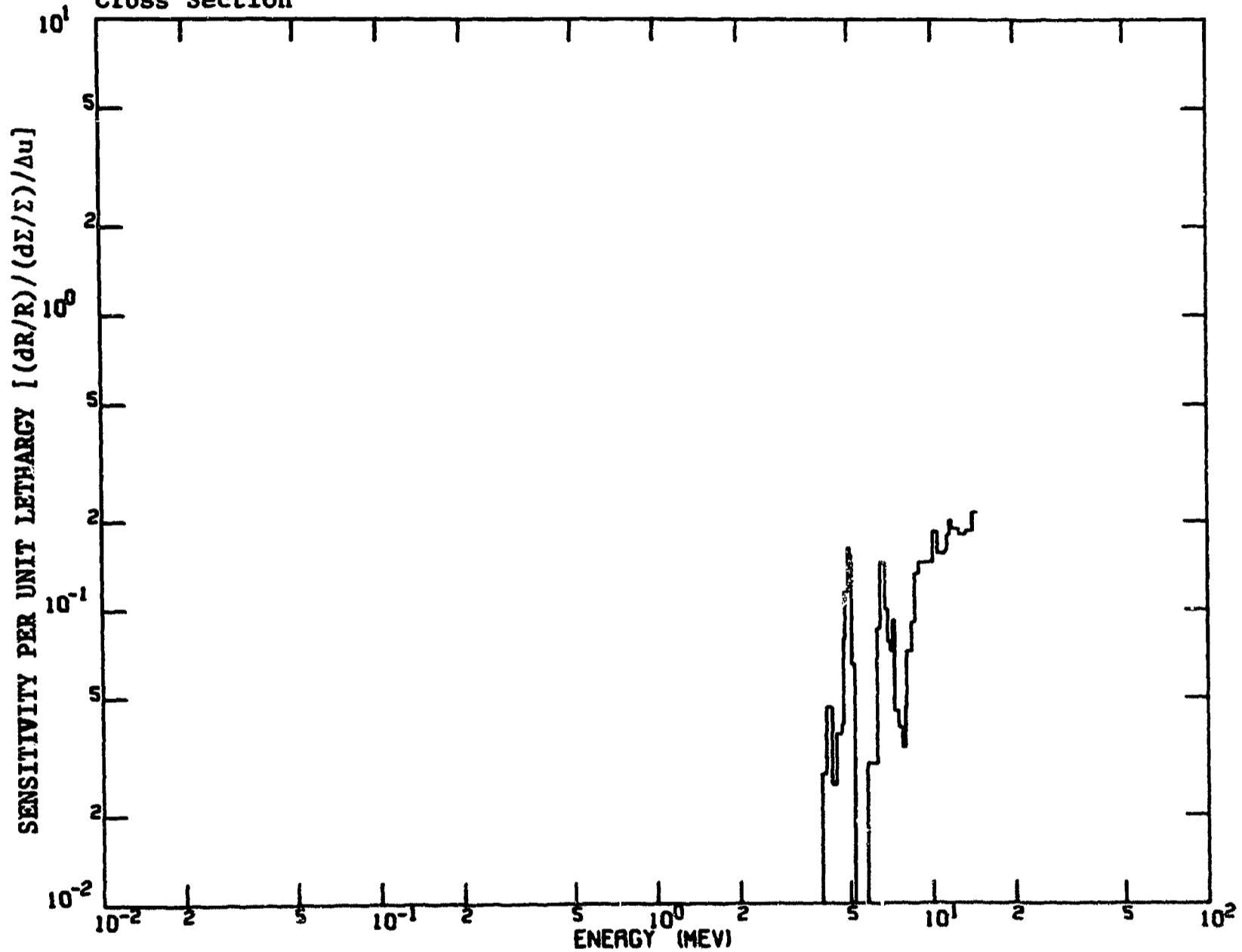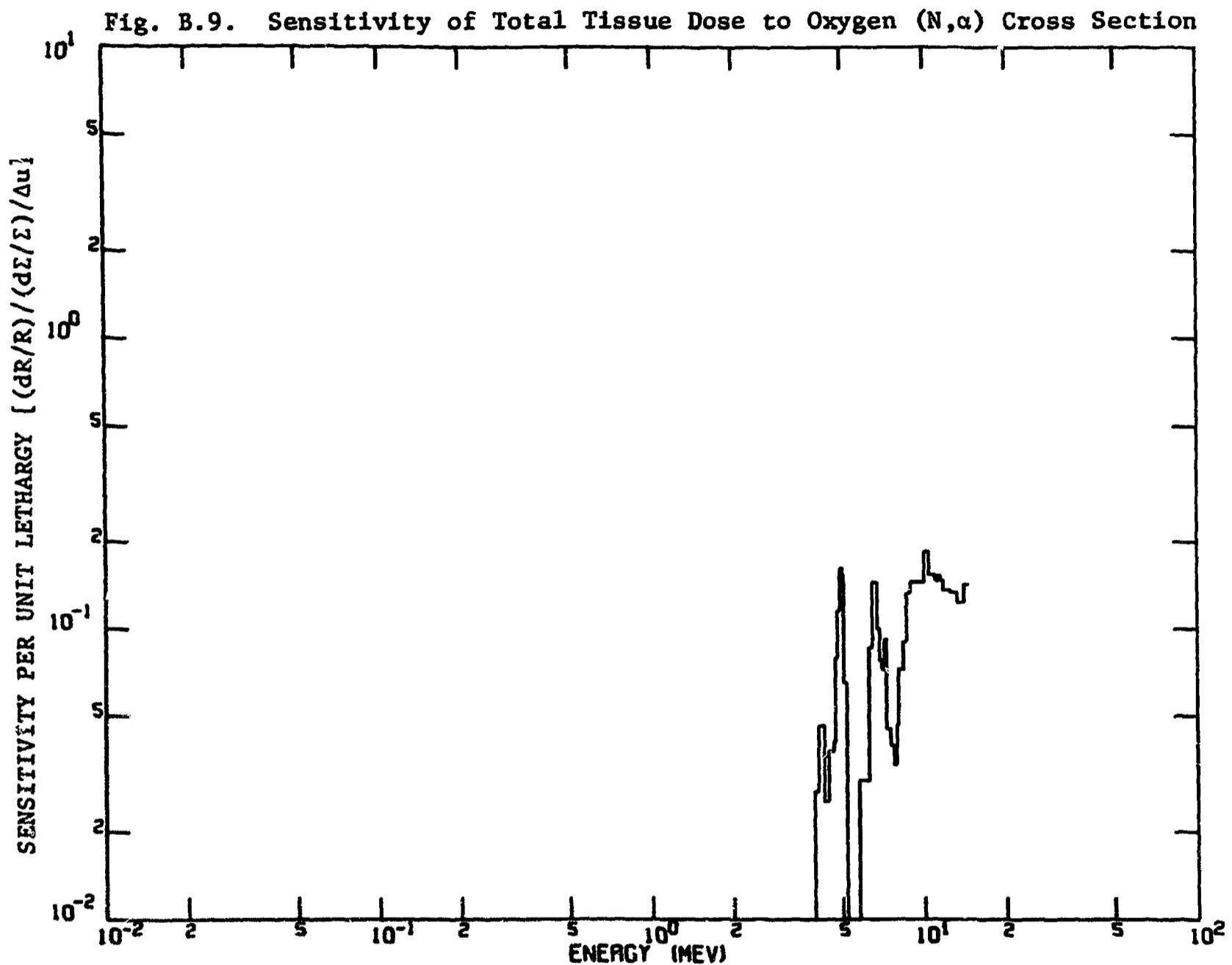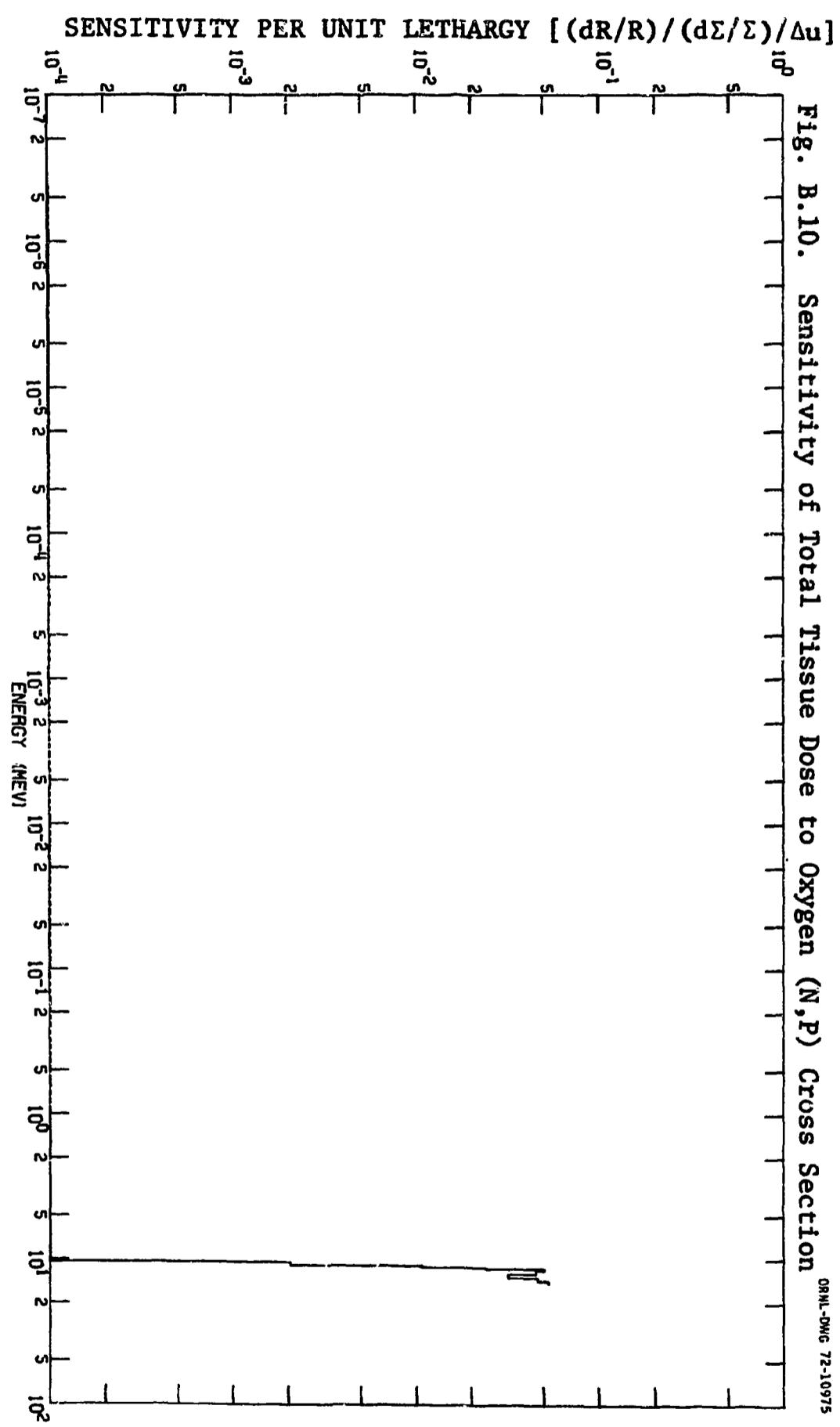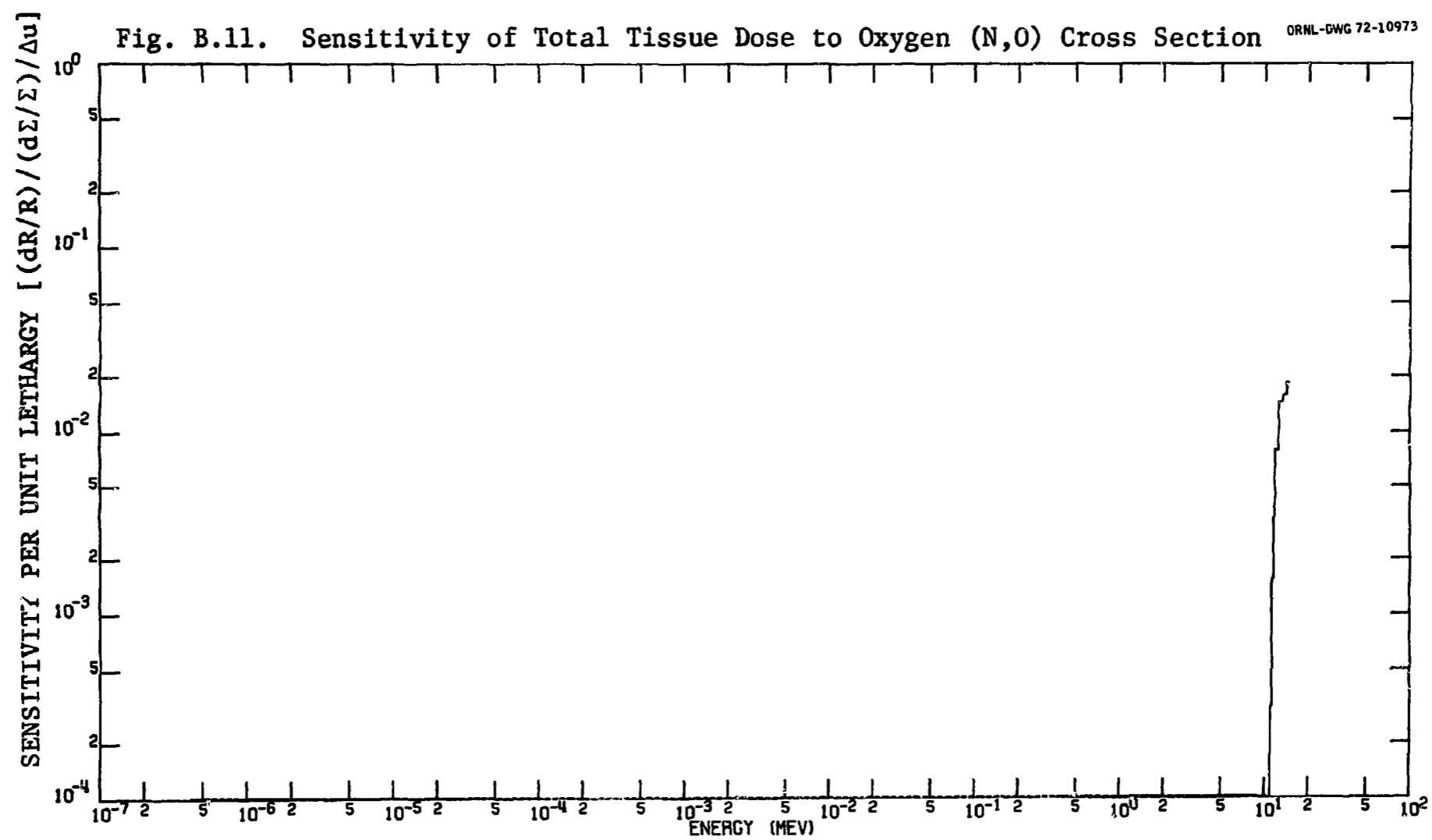
ORNL-DWG 73-4573

Fig. B.12. Sensitivity of Total Tissue Dose to Oxygen Gamma Total Cross Section
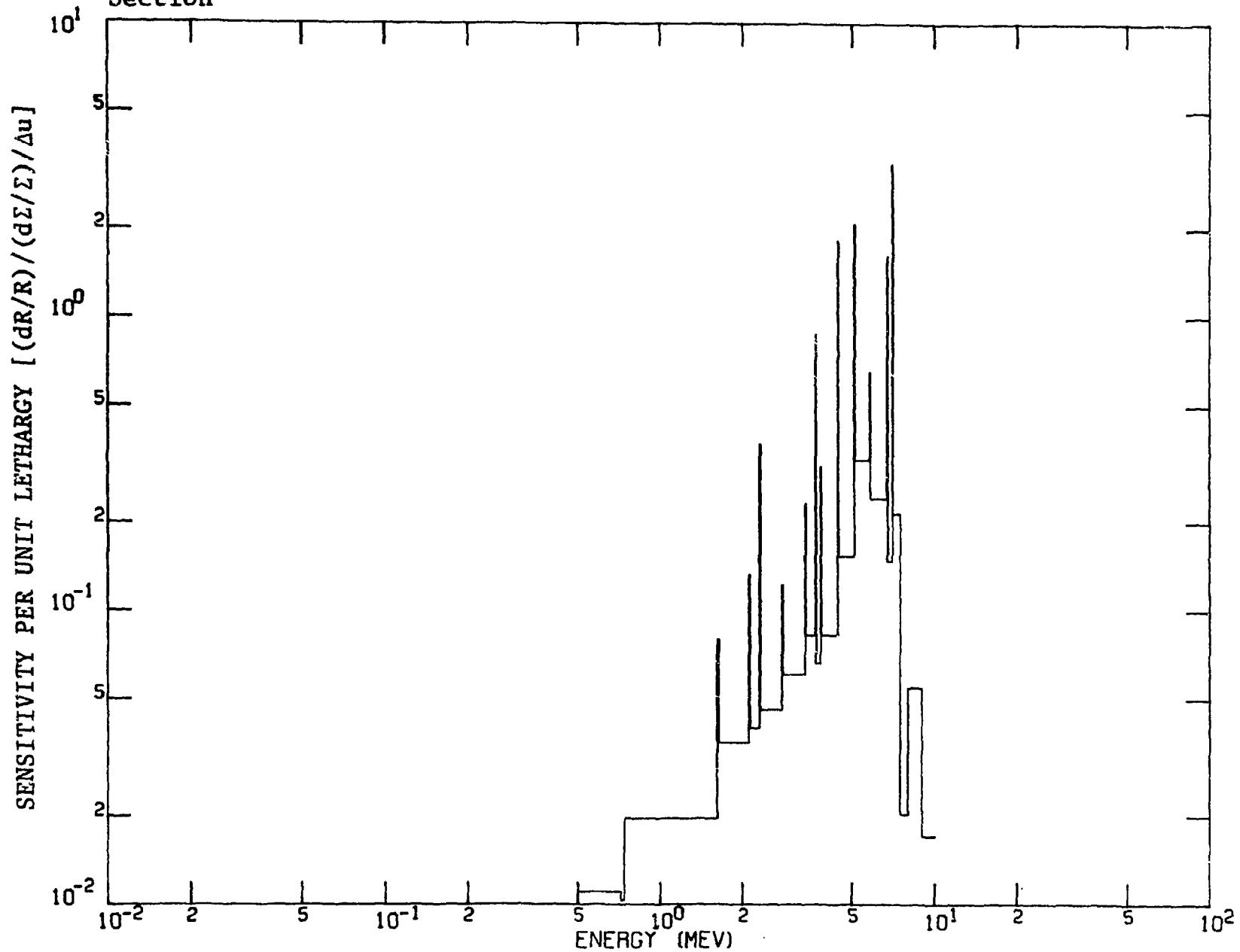
73

ACKNOWLEDGMENTS

REFERENCES

1. E. M. Oblow, "General Sensitivity Theory for Radiation Transport," ORNL-TM-4110 (1973).

2. D. E. Bartine, E. M. Oblow, and F. R. Mynatt, "Neutron Cross-Section Sensitivity Analysis: A General Approach Illustrated for a Na-Fe System," ORNL-TM-3944 (1972).

3. D. R. Marr and J. A. Figg, "Accommodation of Uncertainties in Shield Design," HEDL-TME 72-79, Hanford Engineering Development Laboratory (1972).

4. A. Gandini, "A Generalized Perturbation Method for Bi-linear Functionals of the Real and Adjoint Neutron Fluxes, *J. Nucl. Energy*, *21*, 755 (1967).

5. W. M. Stacey, Jr., "Variational Estimates of Reactivity Worths and Reaction Rate Ratios in Critical Nuclear Reactors, *Nuclear Science and Engineering, 48, 444* (1972).

6. E. Greenspan, "On the Calculation of Reactivity Worths in Fission Reactors," MATT-944, Princeton Plasma Physics Laboratory (1972).

7. R. Conn and W. M. Stacey, Jr., "Variational Methods for Controlled Thermonuclear Reactor Blanket Studies," *Nuclear Fusion* (1973).

8. D. E. Bartine, R. G. Alsmiller, Jr., E. M. Oblow, and F. R. Mynatt, "Cross-Section Sensitivity of Breeding Ratio in a Fusion-Reactor Blanket," ORNL-TM-4208, Oak Ridge National Laboratory (1973).

9. G. E. Hansen and H. A. Sandmeier, "The Effect of Basic Neutron Reaction Cross Sections of Nitrogen (n,n'), (n,2n), (n,γ), (n,p), and (n,α) on High Energy Neutron Penetration in Air," LA-3810, Los Alamos Scientific Laboratory (1967).

10. E. A. Straker, "Sensitivity of Neutron Transport in Oxygen to Various Cross-Section Sets," ORNL-TM-2252 (1968).

11. W. E. Preeg, "Flux Sensitivity to Cross-Section Data for Iron and Oxygen," Doctoral Thesis, Columbia University (1970)

12. S. Hui, D. Spielberg, H. Steinberg, E. S. Troubetzkoy, and M. Kalos, "SAMCEP: An Application of Correlated Monte Carlo to the Simultaneous Solution of Multiple, Perturbed, Time-Dependent Neutron Transport Problems on Complex Three-Dimensional Geometry," BRL-CR-62, Ballistic Research Laboratories, Aberdeen Proving Ground (1972).

13. L. N. Usachev, "Perturbation Theory for the Breeding Ratio," *J. Nucl. Energy, A/B 18, 571* (1964).

14. P. C. E. Hemment *et al*, "The Multigroup Neutron Transport Perturbation Program DUNDEE," AWRE Report 040/66 (1966).

15. D. L. Prezbindowski and H. A. Sandmeier, "The Effects of Cross-Section Inaccuracies on Integral Data," *Trans. Am. Nucl. Soc.,* 193 (1968).

16. J. Lewins, Importance - The Adjoint Function, Pergamon Press, New York (1965).

17. G. I. Bell and S. Gladstone, Nuclear Reactor Theory, Van Nostrand Reinhold Company, New York (1970).

18. E. A. Straker and M. L. Gritzner, "Neutron and Secondary Gamma-Ray Transport in Infinite Homogeneous Air," ORNL-TM-4464 (1969).

19. W. W. Engle, Jr., "A User's Manual for ANISN, A One-Dimensional Discrete Ordinates Transport Code with Anisotropic Scattering," K-1693, Computing Technology Center (1967).

20. D. E. Bartine, F. R. Mynatt, and E. M. Oblow, "SWANLAKE, A Computer Code Utilizing ANISN Transport Calculations for Cross-Section Sensitivity Analysis," ORNL-TM-3809, Oak Ridge National Laboratory (1973).

21. W. S. Snyder and C. Neufeld, *Radiation Research, 6:1,* 67(1957).

22. B. J. Henderson, "Conversion of Neutron and Gamma-Ray Flux to Absorbed Dose Rate," XDC 59-8-179, General Electric Co. (1959).

23. D. E. Bartine, F. R. Mynatt, and E. M. Oblow, "A Sensitivity Analysis of Neutron and Gamma Transport in Air," *Trans. Am. Nucl. Soc., 15,* 959 (1972).

24. F. G. Perey, "A Proposal for Error Quantities in ENDFB/IV," CSEWG Error Subcommittee (1972).

25. P. G. Young and D. G. Foster, Jr., "An Evaluation of the Neutron and Gamma-Ray Production Cross Sections for Nitrogen," Los Alamos Scientific Laboratory, LA 4725 (1972).

26. D. G. Foster, Jr. and P. G. Young, "A Preliminary Evaluation of the Neutron and Photon-Production Cross Sections of Oxygen," Los Alamos Scientific Laboratory, LA-4780 (1972).

27. J. H. Hubbell, "Photon Cross Sections, Attenuation Coefficients, and Energy Absorption Coefficients from 10 KeV to 100 GeV," National Bureau of Standards, NSRDS-NBS-29 (1969).